Precise Adjustement of Nanometric-Scale Diffusion Layers within a Redox Dendrimer Molecule by Ultrafast Cyclic Voltammetry: An Electrochemical Nanometric Microtome

Christian Amatore,*[a] Yann Bouret,[a] Emmanuel Maisonhaute,[a] Jonas I. Goldsmith,[b] and Héctor D. Abruña*[b]

Abstract: Performing cyclic voltammetry at scan rates into the megavolt per second range allows the exploration of the nanosecond time scale as well as the creation of nanometric diffusion layers adjacent to the electrode surface. This latter property is used here to adjust precisely the diffusion layer width within the outer shell of a fourth-generation dendrimer molecule decorated by 64 $[Ru^{II}(tpy)_2]$ redox centers (tpy = terpyridine). Thus the shape of the dendrimer molecule adsorbed onto the ultramicroelectrode surface can be explored voltammetrically in a way reminiscent of an analysis with a nanometric microtome. The quantitative analysis developed here applied to the experimental voltammograms demonstrates that in agreement with previous scanning tunneling microscopy (STM) studies the adsorbed dendrimer molecules are no more spherical as they are in solution but resemble more closely hemispheres resting onto the electrode surface on their diametrical planes. The same quantitative analysis gives access to the apparent diffusion coefficient featuring electron hopping between the $[Ru^{II}/Ru^{III}(tpy)_2]$ redox centers distributed on the dendrimer surface. Based on the electron hopping rate constant thus measured and on a Smoluchowski-type model developed here to take into account viscosity effects during the displacement of the $[Ru^{II}/Ru^{III}(tpy)_2]$ redox centers around their equilibrium positions, it is shown that the $[Ru^{II}/Ru^{III}(tpy)_2]$ redox centers are extremely labile in their potential wells so that they may cross-talk considerably more easily than they would do in solution at an equivalent concentration.

Keywords: cyclic voltammetry · dendrimers · diffusion · electron hopping · N ligands · ruthenium

Introduction

In electrochemical kinetics, the time scale θ of an experiment is given by the duration of diffusion of the molecules under investigation from the electrode surface to the extremity of the diffusion layer. In typical electrokinetic experiments, this property is used to adjust the electrochemical time scale to the half-life $\tau_{1/2}$ of a chemical event to be measured. The interplay between θ and $\tau_{1/2}$ (i.e., $\theta \ll \tau_{1/2}$, $\theta \gg \tau_{1/2}$, and $\theta \approx \tau_{1/2}$) gives rise to distinct and characteristic responses which has made for the widespread use of such techniques.[1]

In cyclic voltammetry, changing the scan rate v allows one to control the thickness of the diffusion layer ($\delta \propto (DRT/Fv)^{1/2}$), so that the duration of diffusion, $\theta \approx RT/Fv$ may be adjusted at will, at least within the experimental limits within which the scan rate may be varied. As v becomes large, the observed response is increasingly affected by the cell's time constant and by ohmic drops within the solution.[2] Both of these effects can be minimized by performing electrochemistry at disk ultramicroelectrodes since, in transient voltammetry, both of the above-mentioned effects are proportional to the electrode radius.[2] Thus, exploration of time scales below a microsecond requires additional diminution of their contributions. We have shown that electronic compensation of the cell resistance, through positive feedback, allows the recording of almost undistorted voltammograms (by using disk ultramicroelectrodes) for sweep rates in the $MV\,s^{-1}$ regime.[3, 4] Accessing this range of scan rates allows the building up of diffusion layers of a few nanometers in thickness near an electrode surface, and therefore access to the nanosecond time scale in electrochemistry.[5]

[a] Dr. C. Amatore, Y. Bouret, E. Maisonhaute
Ecole Normale Supérieure, Département de Chimie
UMR CNRS 8640 "Pasteur"
24 rue Lhomond, 75231 Paris Cedex 05 (France)
Fax: (+33) 1-44-32-38-63
E-mail: amatore@ens.fr

[b] Dr. H. D. Abruña, J. I. Goldsmith
Department of Chemistry, Baker Laboratory
Cornell University
Ithaca, NY 14853-1301 (USA)
Fax: (+1) 1-607-255-9864
E-mail: hda1@cornell.edu

 © WILEY-VCH Verlag GmbH, D-69451 Weinheim, 2001 0947-6539/01/0710-2206 $ 17.50+.50/0

It is also evident that performing voltammetry in the megavolt-per-second range allows one to develop diffusion layers over an electroactive nanometric object adsorbed onto an electrode surface. In such a case and for sufficiently slow scan rates such that the diffusion layer $\delta \propto (DRT/Fv)^{1/2}$ extends much farther than the dimension l of the nanometric object, all the electroactive sites borne by the object are electrolyzed during a single voltammetric scan so that the voltammetric response is that anticipated for a thin adsorbed layer of electroactive material.[6] Conversely, for very fast sweep rates such that $\delta \propto (DRT/Fv)^{1/2} \ll l$, one expects to see a semi-infinite diffusion response, since the physical extremity of the object is not reached by the diffusion layer within the time elapsed during one voltammetric scan. Furthermore, the diffusional voltammetric pattern observed reflects, necessarily, the shape of the space in which diffusion occurs.[2] Thus, one should be able to analyze the shape and dimensions of a nanometric object bearing redox sites adsorbed onto a metallic surface, through the voltammetric patterns observed upon varying the scan rate to values in the megavolt-per-second range, or more generally, when the diffusion layer (controlled by the sweep rate) is smaller than the dimensions of the object under study.

Herein, we illustrate this concept, both theoretically and experimentally, with adsorbed redox-active dendrimers of nanometric dimensions.[6–8] We have previously shown that globular dendrimers bearing redox sites on their outer surface adsorb strongly onto electrode surfaces.[6–13] The adsorptive thermodynamics and kinetics have been extensively characterized by cyclic voltammetry at slow sweep rates coupled to the quartz microbalance (EQCM),[6] as well as by scanning tunneling microscopy (STM).[7, 14] However, STM images only provide the structure of the material exposed to the solution side, but not the contact angle which is hidden under the globular structure exposed to the solution. In this respect, we are interested in examining if a precise analysis of the voltammetric pattern as a function of scan rate carries sufficient information to perform such a shape reconstruction.

On the other hand, being able to restrict diffusion within a single dendrimer structure is expected to allow the determination of the (apparent) diffusion coefficient corresponding to the propagation of the electrochemical perturbation along its surface. Since the redox centers are physically bound to the radial molecular branches of the dendritic structure, they are not expected to be able to diffuse in the classical Einstein–Schmoluchowski sense. In fact, a similar problem was addressed several years ago for diffusion in macroscopic polymeric films containing covalently linked redox sites.[15–22] In this context, an apparent diffusion coefficient (D_{app}) is observed, which corresponds to an apparent displacement of redox centers by electron hoping between them. Thus, the electrochemical perturbation may propagate along the structure without implying any real displacement of each redox site (at least in terms of their average displacement). Therefore, the measurement of such an apparent diffusion coefficient along the electroactive outer shell of a dendrimer carries information on the degree of cross talk between groups located at the end of the dendrimer chains.[21, 22] Here, by construction, we examine such redox communication. However, as will be made evident in the following, the communication depends on two factors independent of the chemical nature of the cross-talk between adjacent sites. One relates to the rate constant characterizing the chemical exchange between two sites, and is, ultimately, controlled by the rate constant characterizing the same exchange in a bulk solution of sites. The other characterizes the degree of communication between adjacent sites and is therefore expected to be intrinsic to the dendrimer's inner structure and thus rather independent of the chemical reaction leading to the cross-exchange of status between two adjacent sites. In view of the expected important properties of redox-active dendrimers in catalysis,[23–35] accessing such information appears as a valuable and important challenge. It also has important conceptual interest.

Theory

We consider that the dendrimer adsorbs onto the electrode surface as a spherical globular structure since this is what is apparent from STM images of these dendrimers.[7] These materials adsorb so strongly to electrode surfaces at very low (nanomolar) bulk concentrations in acetonitrile that any motion (viz., rotation or rotational oscillation) is ruled out.[6–8] Since the monomeric $[Ru(tpy)_2]^{2+}$ ion is quite soluble in acetonitrile, the strong adsorption is a clear indication of the strong preference of the dendrimer chains, linking the redox sites to the dendrimer center, for the electrode surface relative to the solvent molecules. Adsorption to high coverage values creates a steric problem, so it is presumed that upon adsorbing, the dendrimer molecule optimizes its configuration so that the negative energy of adsorption (over)compensates for the positive steric energy.[8] This is expected to result in a distortion of the dendrimer shape with respect to the spherical shape it retains in solution.[36–38] Similarly, since access to the solvent molecules in between the chains has to be minimized for the entire structure exposed to the solution, it is expected that the average cone angle, occupied by one redox site, seen from the dendrimer center, is rather constant. In this perspective, the adsorbed dendrimer should resemble a truncated sphere of radius R_0 resting on the electrode surface so that the truncated part of the sphere is confined within the cone of half-angle φ_0 (see Figure 1 a). This angle is imposed by

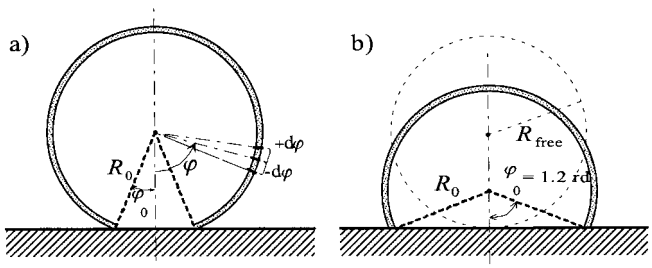

Figure 1. a) Schematic representation of a dendrimer adsorbed onto the electrode surface in which the definitions of φ_0, R_0, and φ are denoted. The redox centers are considered to move only in the gray shell around the inner core of the dendrimer. b) Schematic representation of the adsorbed dendrimer for $\varphi_0 = 1.2$ rd. In b) the dashed circle represents the size of the same dendrimer free in solution, assuming that the two inner volumes are equal.

the compensation of positive (steric) and negative (adsorption) energies. The N_0 redox sites are disposed within a spherical shell at the surface of this globule, of thickness d, equal to the diameter of the spherical volume occupied by one redox site. Since N_0 redox sites are distributed on a surface area $2\pi R_0^2(1+\cos\varphi_0)$, their molecular surface concentration (in moles per unit of surface area of the dendrimer outer shell) is $\Gamma_0 = N_0/[2\pi R_0^2(1+\cos\varphi_0)]$, so that their average molecular concentration (in moles per unit of volume) is $C_0 = \Gamma_0/d$, within the spherical shell in which they are distributed.

In the experiments performed in this study, $N_d = \pi r_0^2 \Gamma_d N_A$ redox dendrimers are adsorbed on a disk electrode of radius r_0 with a surface concentration Γ_d (where N_A is Avogadro's constant and Γ_d is expressed in moles per unit of surface area of the electrode). However, each dendrimer behaves independently since they are adsorbed too far apart to communicate through electron transfer,[7] so that the voltammograms observed ought to be the simple superposition of each individual voltammogram. Whenever the distribution of shapes is extremely narrow (vide infra), each dendrimer should behave identically so that the voltammetric current would be expected to be N_d times that of one dendrimer. For this reason, hereafter we consider only a single dendrimer molecule.

Apparent diffusion by electron hopping within a spherical shell of redox sites: The following model is adapted from that derived previously for planar diffusion through electron hopping in electroactive polymers,[15–22, 39, 40] so its only particularities deal with the specific geometry of the system at hand. In the outer shell of the dendrimer (see Figure 1) of thickness d, each redox site may be present under two states A and B, which are related through the exchange of n electrons [Eq. (1)].

$$A_{site1} + ne \rightleftharpoons B_{site1} \tag{1}$$

We note that $\Gamma_A = C_A d$ is the molecular surfacic concentration of species A, so that the surfacic molecular concentration of species B is $\Gamma_B = \Gamma_0 - \Gamma_A = (C_0 - C_A)d$ at the same location. Let us then consider two rings of the spherical shell, parallel to the electrode surface and located around the latitude φ (see Figure 1a). The redox sites contained in each of these two adjacent rings may exchange n electrons with those of the neighboring ring [Eq. (2)].

$$A_{site1} + B_{site2} \rightleftharpoons B_{site1} + A_{site2} \tag{2}$$

The rate constant k of this electron exchange is identical for each half-reaction (2) owing to the symmetry. Indeed, since the redox sites are distributed over a shell of redox sites that is surrounded externally by the electrolyte at high concentration, we may neglect electric field contributions due to the site exchanges so that $\Delta G^0 = 0$ for Equation (2).[41] In other words, we assume here that the concentrations (0.6 M in the experiments reported here, vide infra) and mobilities of the inert supporting electrolyte ions in the surrounding solution are sufficiently large to maintain electroneutrality at each instant.[41] Furthermore, under such highly concentrated supporting electrolyte concentrations conditions the double layer thickness is of a few angstroms only so that the charges are effectively screened.[1] Under these conditions, the apparent movement of A from site 1 to site 2 as featured in Equation (2) is controlled only by the rate of diffusion by electron hoping.[42] Note that we assume here that the rate of electron tunneling from centers distributed on the outer shell of the dendrimer and the electrode is negligible in view of the electron hopping process (vide infra).

Let us then consider two spherical rings of thickness $R_0\delta\varphi$ located around the latitude φ (see Figure 1a), of elementary volumes $2\pi R_0(\sin\varphi)d\delta\varphi$, and separated by the surface area $a = 2\pi R_0(\sin\varphi)d$ normal to the spherical shell. During the time interval δt, the apparent flux of sites A along the φ coordinate, $J_{A,\varphi}$, resulting from the net effect of the forward and backward electron exchanges in Equation (2) is given in Equation (3), where δN_A is the net number of moles of sites A created in the volume comprised between φ and $\varphi + \delta\varphi$ during δt.

$$J_{A,\varphi} = \delta N_A/(a\delta t) \tag{3}$$

δN_A is then given by Equation (4).

$$\frac{\delta N_A}{(aR_0\delta\varphi)} = k\delta t\left[C_A\left(\varphi - \frac{\delta\varphi}{2}\right)C_B\left(\varphi + \frac{\delta\varphi}{2}\right) - C_A\left(\varphi + \frac{\delta\varphi}{2}\right)C_B\left(\varphi - \frac{\delta\varphi}{2}\right)\right] \tag{4}$$

Since $C_B = (C_0 - C_A)$, development of Equation (4), gives rise to the net flux [Eq. (5)] and [Eq. (6)].

$$J_{A,\varphi} = \frac{\delta N_A}{(a\delta t)} = kC_0\left[C_A\left(\varphi - \frac{\delta\varphi}{2}\right) - C_A\left(\varphi + \frac{\delta\varphi}{2}\right)\right]R_0\delta\varphi \tag{5}$$

that is:

$$J_{A,\varphi} = -kC_0(R_0\delta\varphi)^2\left[\left(\frac{1}{R_0}\right)\left(\frac{\partial C_A}{\partial\varphi}\right)_\varphi\right] = -kC_0(R_0\delta\varphi)^2\mathrm{grad}_\varphi C_A \tag{6}$$

In Equation (6) $\mathrm{grad}_\varphi C_A$ is the projection of the gradient of C_A along the φ spherical coordinate. $kC_0(R_0\delta\varphi)^2$ has the dimensions ($[L^2][T^{-1}]$) and the physical meaning of a diffusion coefficient in the Einstein–Schmoluchowski sense. Indeed, it corresponds to an equivalent displacement of A particles over the length $R_0\delta\varphi$ during the time interval $\delta t = 1/(2kC_0)$. Therefore, Equation (6) shows that the electron exchange in Equation (2) amounts to an equivalent diffusion of A sites over the spherical shell with an equivalent diffusion coefficient (note that $C_0 = \Gamma_0/d = N_0/[2\pi R_0^2 d(1+\cos\varphi_0)]$; Eq. (7)).[15–22, 39, 40, 42]

$$D_{hop} = kC_0(R_0\delta\varphi)^2 = k\Gamma_0\frac{(R_0\delta\varphi)^2}{d} = \left(\frac{N_0}{2\pi}\right)\frac{[k(\delta\varphi)^2/d]}{1+\cos\varphi_0} \tag{7}$$

Meaning of D_{hop} within a spherical shell of redox sites: A single site occupies an average surface area $\delta a_{site} = 2\pi R_0^2(1+\cos\varphi_0)/N_0$ of the spherical shell, which corresponds to an average angular distance $\delta\varphi_{site} = 2\arccos[1-(1+\cos\varphi_0)/N_0]$ between the centers of two sites, that is, to $\delta\varphi_{site} \approx 2^{3/2}[(1+\cos\varphi_0)/N_0]^{1/2}$ to better than 3% for N_0 larger than ten. In practice, in order to allow the propagation of the electrochemical perturbation, one must have $\delta\varphi = \delta\varphi_{site}$ in Equation (7) so that Equation (8) is valid.

$$D_{hop} = (4/\pi)k/d \tag{8}$$

© WILEY-VCH Verlag GmbH, D-69451 Weinheim, 2001
0947-6539/01/0710-2208 $ 17.50+.50/0 *Chem. Eur. J.* **2001**, *7*, No. 10

In Equation (8) k is the apparent rate constant of electron transfer between two sites located at an average distance $R_0\delta\varphi_{site}$ and which results in the propagation of the electrons in the $+\delta\varphi$ direction. When N_0 is sufficiently large for $R_0\delta\varphi_{site}$ to be close to d, that is, when $N_0 = N_{max} \approx 8(1+\cos\varphi_0)(R_0/d)^2$, all the sites are in close contact. Then, $k \approx k_{act}^{soln}/6N_A$, where k_{act}^{soln} is the molar isotopic activation rate constant determined for the same redox centers in a homogeneous bulk solution giving rise to a similar environment of the redox centers. The factor 1/6 is introduced because in a three-dimensional bulk solution reactions may occur along the two directions of the three coordinates while here, no reaction is feasible along the radial spherical coordinate (that is, $\pm\delta r$), whereas electron transfers occurring along the longitudinal coordinate (that is, $\pm\delta\theta$) or along the negative direction of the φ coordinate do not contribute to the flux evaluated above. Thus only one event over the six feasible in solution is to be retained, so that Equation (9) is valid.

$$D_{hop} = (D_{hop})_{max} = (2/3\pi d N_A) k_{act}^{soln} \quad (9)$$

$R_0\delta\varphi_{site} = d(N_{max}/N_0)^{1/2}$ provided that N_0 is larger than about ten as mentioned above. Thus, when $N_0 < N_{max}$, in their equilibrium location, the sites exchanging electrons are separated by a distance that exceeds their close contact center-to-center distance. As a result, since the sites are assumed be pinned at their equilibrium location on the spherical shell, the rate of electron transfer decreases relative to the above value because of the smaller overlap, between their orbitals, during the very act of electron transfer. A precise evaluation of the ensuing decay of k would require quantum calculations which are beyond our purpose and scope. However, several studies on long-range electron transfer point out that under such conditions, k drops exponentially with the distance $d^{\#} = R_0\delta\varphi_{site} - d = d[(N_{max}/N_0)^{1/2} - 1]$ between the two centers at the transition state [Eq. (10)].[43–45]

$$k = k_{pin} = (k_{act}^{soln}/6N_A)\exp(-\lambda d^{\#}) = (k_{act}^{soln}/6N_A)\exp\{-\lambda d[(N_{max}/N_0)^{1/2} - 1]\} \quad (10)$$

In Equation (10) λ is the attenuation factor per unit of distance. This is generally on average 1 Å^{-1}, that is, 10 nm^{-1},[44, 45] and larger than 0.5 Å^{-1}, that is, 5 nm^{-1}, for nonconducting linkers. It then follows that Equation (11) is valid.

$$D_{hop} = (D_{hop})_{pin} = (D_{hop})_{max}\exp\{-\lambda d[(N_{max}/N_0)^{1/2} - 1]\} \quad (11)$$

Equation (9), where $(D_{hop})_{max}$ is defined, applies only when the sites are pinned at their equilibrium position on the spherical shell. However, they may experience fluctuating displacements from their equilibrium position, due to partial flexibility of their linkers. In doing so, they may become closer, and exchange an electron, faster than predicted by Equation (10). However, this is done by increasing the site potential energy in its potential well centered at its equilibrium position. If one assumes that the sites may sample their individual potential wells much faster than the rate of electron transfer, that is, that their potential well is populated with a Boltzmann distribution, the overall rate constant is given by Equation (12).

$$k = \left[\frac{k_{act}^{soln}(W_A - W_B)}{6N_A}\right]\exp[-\lambda(R_0\delta\varphi_{site} - d - x_A - x_B)]\exp-\left[\frac{(W_A + W_B)}{k_B T}\right] \quad (12)$$

In Equation (12), x_A and x_B are the displacements of each site A and B from their equilibrium position at the very moment of electron transfer. W_A and W_B are the free energies due to the displacements x_A and x_B of either site in their respective potential wells, and $k_{act}^{soln}(W_A - W_B)$ is the solution activation rate constant at the driving force $\Delta G^{\#} = W_A - W_B$ which prevails at the moment of electron transfer (k_B is the Boltzmann constant). Since the orbital coupling is maximized when $W_A = W_B$, that is, $x_A = -x_B$, in the following we will examine only this situation which corresponds to an antisymmetric displacement of each site. Then Equation (12) becomes Equation (13).

$$k(x^{\#}) = k_{pin}\exp(2\lambda x^{\#})\exp[-2W(x^{\#})/k_B T] \quad (13)$$

In Equation (13) $x^{\#}$ is the common value of the displacements. The first exponential term increases with $x^{\#}$, while the second one decreases because $W^{\#}(x^{\#})$ increases. This shows that k passes through a maximum when $x^{\#}$ varies between 0 (each site being at its equilibrium position) to $x_{max} = (R_0\delta\varphi_{site} - d)/2$ (each site being in close contact). The position of this maximum depends on λ as well as on the potential energy $W(x)$. To evaluate this maximum, let us assume that the potential wells of each site are harmonic with a strength constant κ, that is, that $W(x) = \kappa x^2/2$. The optimum value of $x^{\#}$, $x_{opt}^{\#}$, corresponds then to $dk(x^{\#})/dx^{\#} = 0$, that is, to Equation (14), whenever $x_{opt}^{\#} \le x_{max}$, that is for $2\lambda k_B T/\kappa \le (R_0\delta\varphi_{site} - d) = d[(N_{max}/N_0)^{1/2} - 1]$, or to $x_{opt}^{\#} = x_{max} = d[(N_{max}/N_0)^{1/2} - 1]/2$ in the reverse situation.

$$x_{opt}^{\#} = \lambda k_B T/\kappa \quad (14)$$

One then obtains Equation (15).

$$k(x_{opt}^{\#}) = k_{max}\exp[-(\kappa d^2/4k_B T)[(N_{max}/N_0)^{1/2} - 1]^2] \quad (15)$$

This can be converted into Equation (16) when $N_0 \ge N_{max}/(1+2\lambda k_B T/\kappa d)^2$, that is, at large coverage of redox sites.

$$(D_{hop})_{opt} = (D_{hop})_{max}\exp[-(\kappa d^2/4k_B T)[(N_{max}/N_0)^{1/2} - 1]^2] \quad (16)$$

Alternatively, one obtains [Eq. (17)].

$$k(x_{opt}^{\#}) = k_{pin}\exp(\lambda^2 k_B T/\kappa) \quad (17)$$

This can be converted to Equation (18) when $N_0 \le N_{max}/(1 + 2\lambda k_B T/\kappa d)^2$, that is at low coverage of redox sites.

$$(D_{hop})_{opt} = (D_{hop})_{max}\exp\{-(\lambda^2 k_B T/\kappa)[(\kappa d/\lambda k_B T)[(N_{max}/N_0)^{1/2} - 1] - 1]\} \quad (18)$$

Thus, the value of D_{hop} at the optimum distance depends on two dimensionless parameters, $\lambda^2 k_B T/\kappa$, and $\sigma = (\kappa d/2\lambda k_B T)[(N_{max}/N_0)^{1/2} - 1]$. Indeed, Equations (16) and (18) may be rewritten as a function of these parameters in the

form of Equation (19) when $\sigma \leq 1$, that is, when $N_0 \geq N_{max}/(1+2\lambda k_B T/\kappa d)^2$, that is, at large coverage of redox sites.

$$D_{hop} = (D_{hop})_{max}\exp[-(\lambda^2 k_B T/\kappa)\sigma^2] \quad (19)$$

Alternatively, it may be rewritten in the form of Equation (20) when $\sigma \geq 1$, that is, $N_0 \leq N_{max}/(1+2\lambda k_B T/\kappa d)^2$, that is at low coverage of redox sites.

$$D_{hop} = (D_{hop})_{max}\exp[-(\lambda^2 k_B T/\kappa)(2\sigma - 1) \quad (20)$$

As noted in Figure 2, these two functions join without discontinuity at $\sigma = 1$, so that the variations of D_{hop} with σ are continuous despite the two different formulations. Furthermore, these equations encompass the entire range of possibilities considered up to here. Indeed, when $\sigma \to 0$, that is, when $N_0 \to N_{max}$, Equation (19) shows that $D_{hop} \to (D_{hop})_{max}$ [Eq. (9)]. Note that the same also occurs when $(\lambda^2 k_B T/\kappa)\sigma^2 \to 0$, that is, whenever the sites are sufficiently loose around their equilibrium positions that their displacements, in their potential wells over the distance $(R_0\delta\varphi_{site} - d)$ required for performing an electron transfer at $k = k_{act}^{soln}/6$, do not introduce any appreciable energetic cost. In the converse situation, that is, when $\sigma \to \infty$, either because $N_0 \ll N_{max}$ and/or because $\kappa \to \infty$, that is, when the redox sites are very diluted on the spherical shell and rigidly pinned at their equilibrium position, Equation (20) shows that $D_{hop} \to (D_{hop})_{pin}$ [Eq. (11)]. In other words, Equations (19) and (20) describe any situation which may arise within the framework considered up to here provided that one assumes that percolation[21, 22] is not significant and that the sites experience a Boltzmann distribution in their potential wells independent of the rate of electron transfer.

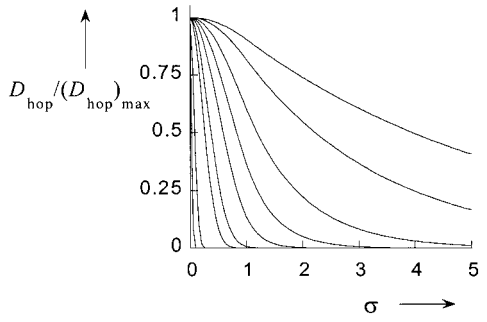

Figure 2. Variations of $D_{hop}/(D_{hop})_{max}$ as a function of σ [Eqs. (19) or (20)] (see text) for different values of $\lambda^2 k_B T/\kappa$. From top to bottom, $\lambda^2 k_B T/\kappa = 0.1$, 0.2, 0.5, 1, 2, 5, 10, 100, and 1000.

To evaluate D_{hop} in Equations (19) and (20), we assume that the sites are in thermal equilibrium in their potential wells. This implies that the rate of population of the different energy levels by the redox sites in their potential wells is infinitely large relative to the overall rate of electron transfer at the optimum value, $x^{\#}$. When this is not the case, the rate of viscous displacement of the sites in their wells may become the limiting step.[46] To evaluate this situation, we proceed as follows. First, we define a *pseudo*-particle composed of a pair of reacting A and B sites, shifted respectively by x_A and x_B from their equilibrium positions in two adjacent potential wells. For simplification of the following derivations, we impose again a condition of anti-symmetry for the two displacements (that is, $|x_A| = |x_B| = x$) although in reality these are independent variables. By doing so we suppress the possible occurrence of percolation.[21, 22] Let $\Gamma(x)$ be the surfacic concentration of this pseudo-particle $\{A\cdots B,x\}$. Then, the overall rate of electron transfer is given by Equation (21) where N is the number of pseudo-particles, and $x^{\#}$ is the location where the electron transfer takes place at a rate constant $k^{\#}$.

$$dN/dt = -k^{\#}\Gamma(x^{\#})/d \quad (21)$$

The rate constant $k^{\#}$ is given by Equation (22).

$$k^{\#} = k_{act}^{soln}\exp[-\lambda(R_0\delta\varphi_{site} - d - 2x^{\#})] \quad (22)$$

We now need to evaluate $x^{\#}$. When x varies, the chemical potential of the *pseudo*-particle varies according to Equation (23).

$$\mu = \mu_0 + k_B T \ln\Gamma(x) + \kappa x^2 \quad (23)$$

This chemical potential corresponds to a force $F = d\mu/dx$ applied to the *pseudo*-particle. Denoting η_S as the surfacic kinematic viscosity of the particle in its potential well, and assuming complete viscous dissipation of energy, we calculate the local velocity of the particle to be $V(x) = F(x)/(4\pi\eta_S)$, so that its flux $j(x) = \Gamma(x)V(x)/d$ is given by Equation (24).

$$j(x) = (k_B T/4\pi\eta_S d)[d\Gamma(x)/dx + 2(\kappa/k_B T)x\Gamma(x)] \quad (24)$$

The reaction occurring at $x = x^{\#}$ imposes a steady-state flux regime, so that $(2\pi x d)j(x)$ is independent of x and equal to $(2\pi x^{\#} d)j(x^{\#})$, which is imposed by the rate of electron transfer reaction that takes place at $x^{\#}$ according to Equation (25), so that $j(x) = -k^{\#}\Gamma(x^{\#})/(2\pi x d^2)$.[46, 47]

$$dN/dt = -k^{\#}\Gamma(x^{\#})/d = (2\pi x^{\#} d)j(x^{\#}) = (2\pi x d)j(x) \quad (25)$$

Taking this condition into account, the integration of Equation (24) shows that the rate of electron transfer defined with respect to the surfacic concentrations at $x = 0$, that is, by $dN/dt = -k_{ap} \times \Gamma(x = 0)/d$, occurs with an apparent rate constant k_{ap} given by Equation (26).

$$k_{ap}^{-1} = [k^{\#}\exp(\kappa x^{\#2}/k_B T)]^{-1} + (2\eta_S/k_B T d)\int_0^{x^{+}} \exp(\kappa x^2/k_B T)(dx/x) \quad (26)$$

As expected, the formulation in Equation (26) is very reminiscent of the Debye–Schmoluchowski–Noyes formulation,[46–48] with the equivalent of the so-called diffusion limit rate constant being in this case given by Equation (27).

$$k_{visc}(x^{\#}) = k_B T d/\{2\eta_S \int_0^{x^{+}(\kappa/k_B T)^{1/2}} [\exp(u^2)/u]du\} \quad (27)$$

Therefore, using Equation (9), and by considering for the simplification of the following presentation that most of the sites are located near the minima of their potential wells, we

 © WILEY-VCH Verlag GmbH, D-69451 Weinheim, 2001 0947-6539/01/0710-2210 $ 17.50+.50/0 *Chem. Eur. J.* **2001**, *7*, No. 10

finally obtain Equation (28) by considering only one sixth of the events (vide supra).

$$1/D_{hop} = 1/D_{hop}^{\#} + 1/D_{visc}^{\#} \quad (28)$$

Here $D_{hop}^{\#}$ is the activation-controlled contribution to D_{hop} [Eq. (29)] and $D_{visc}^{\#}$ is the viscous-controlled contribution to D_{hop} [Eq. (30)].

$$D_{hop}^{\#} = (D_{hop})_{max}\exp\{-\lambda d[(N_{max}/N_0)^{1/2}-1]\}\exp[2\lambda x^{\#} - \kappa x^{\#2}/k_BT] \quad (29)$$

$$D_{visc}^{\#} = k_BT/\{3\pi\eta_S \int_0^{x^+(\kappa/k_BT)^{1/2}} [\exp(u^2)/u]du\} \quad (30)$$

Equation (28) may be rewritten in the form of Equation (31).

$$D_{hop} = (D_{hop})_{pin}/\{\exp(-2\lambda x^{\#} + \kappa x^{\#2}/k_BT) + \Omega \int_0^{x^+(\kappa/k_BT)^{1/2}} [\exp(u^2)/u]du\} \quad (31)$$

Here $\Omega = 3\pi\eta_S(D_{hop})_{pin}/k_BT$ and $(D_{hop})_{pin}$, defined in Equation (11), corresponds to the value of D_{hop} when the sites are pinned at their equilibrium position. The largest value of D_{hop} corresponds to the value $(x^{\#})_{opt}$ of $x^{\#}$ that minimizes the denominator of Equation (31) provided this is less than or equal to $x_{max} = d[(N_{max}/N_0)^{1/2}-1]/2$, the maximum value of x. As noted before [Eqs. (19) and (20)], when the mathematical solution $(x^{\#})_{opt}$ becomes larger than x_{max}, the largest value of D_{hop} corresponds to $(x^{\#})_{opt} = x_{max}$. It follows that $(x^{\#})_{opt} = Max\{0,Min[z(\lambda k_BT/\kappa),x_{max}]\}$, where z is the largest solution of Equation (32) and $\zeta = 2\lambda^2 k_BT/\kappa$.

$$z(1-z) = (\Omega/\zeta)\exp(\zeta z) \quad (32)$$

When the right-hand-side term of Equation (32) is negligible, one obtains $z = 1$, which features the solution found above by neglecting the role of the viscosity. Then, the optimum value of D_{hop} is given by Equation (19) or (20) depending on the value of σ. This requires that $\Omega(\exp\zeta)/\zeta \to 0$ when $\sigma \le 1$, or $(\Omega/\zeta)\exp(2\lambda x_{max}) \to 0$ when $\sigma \ge 1$. When either condition is not fulfilled, z is smaller than unity or than x_{max}, which shows that D_{hop} is smaller than predicted by Equation (19) or (20), respectively. In other words, the viscosity prevents the sites from reaching the optimum electron transfer point at a sufficiently fast rate. For a given value of ζ, whenever Ω is larger than a threshold value $\Omega_{max}(\zeta) = (1-2\phi)\exp(-\xi\phi)$ where $\phi = [2+\xi+(4+\xi^2)^{1/2}]/(2\xi)$, Equation (32) has no solution so that $(x^{\#})_{opt} = 0$. This means that because of the cumulative effects of work terms and of the viscosity, the sites cross-talk from their equilibrium positions, and therefore $D_{hop} = (D_{hop})_{pin}$. When $\Omega < \Omega_{max}(\zeta)$, the sites may move to be closer at the moment of electron transfer, yet if Ω is not sufficiently small $x^{\#} < (x^{\#})_{opt}$ so that $(D_{hop})_{pin} < D_{hop} < (D_{hop})_{opt}$, where $(D_{hop})_{opt}$ is given in Equation (19) or (20). Therefore, this analysis shows that the possible rigidity of the adsorbed dendrimer structure may play an extremely important role on D_{hop} through its control of the value of Ω and not only through that of $\lambda^2 k_BT/\kappa$.

Fick's first and second laws for apparent diffusion over the spherical shell surface

Since the flux of A sites along the radial and spherical angular coordinates is null by symmetry or by construction, the above results show that the apparent flux of sites A is governed by a law equivalent to Fick's first law describing diffusion into the confined spherical shell [Eq. (33); note that in Equations (33) and (34), bold italic fonts indicate three-dimensional vectors].

$$\boldsymbol{J}_A = -D_{hop}\boldsymbol{grad}C_A \quad (33)$$

By using Equation (33), the universal matter conservation law readily provides an equivalent to Fick's second law as given in Equation (34), where Δ is the three-dimensional Laplacian.

$$\partial C_A/\partial t = -\mathrm{div}\boldsymbol{J}_A = D_{hop}\mathrm{div}(\boldsymbol{grad}C_A) = D_{hop}\Delta C_A \quad (34)$$

Thus, one obtains within the confined shell given in Equation (35), where $f = \Gamma_A/\Gamma_0$ is the local fraction of sites A.

$$\partial f/\partial t = D_{hop}(R_0^2\sin\varphi)^{-1}\partial[(\sin\varphi)(\partial f/\partial\varphi)]/\partial\varphi = (D_{hop}/R_0^2)[\partial^2 f/\partial\varphi^2 + (\partial f/\partial\varphi)/\tan\varphi] \quad (35)$$

Note that Equation (35) has a singularity at $\varphi = \pi$ since $\mathrm{cotan}\varphi \to \infty$ when $\varphi \to \pi$. Since $\partial f/\partial t$ is necessarily finite except at possible time singularities of the electrochemical perturbation, the above singularity implies that $(\partial f/\partial\varphi)_\pi = 0$, a result that follows from the symmetry and topology of the problem.Since the displacement of one site A is equivalent to the reverse displacement of n electrons, the flux in Equation (6) corresponds to the net current intensity flowing through the cross-section of the shell at latitude φ as given by Equation (36).

$$I(\varphi) = neaJ_A = -2\pi ne\Gamma_0 D_{hop}[(\sin\varphi)(\partial f/\partial\varphi)] \quad (36)$$

Note that in Equation (36) we use here the IUPAC convention, so that oxidation ($n < 0$) currents are positive. Noting that Γ_0 corresponds to the homogeneous distribution of N_0 sites over all of the spherical shell except for its flattened section (Figure 1a), one has $\Gamma_0 = N_0/[2\pi R_0^2(1+\cos\varphi_0)]$, so that the current intensity is (note that $\sin\varphi_0/(1+\cos\varphi_0) = \tan(\varphi_0/2)$) is given by Equation (37), where the subscript zero indicates that the value is taken at $\varphi = \varphi_0$ (this convention is observed throughout the remainder of the text).

$$I = -neN_0(D_{hop}/R_0^2)\tan(\varphi_0/2)(\partial f/\partial\varphi)_0 \quad (37)$$

Equation (37) has the feature that when $\varphi_0 \to 0$, $\tan(\varphi_0/2) \sim (\varphi_0/2) \to 0$, so that a finite current corresponds to an infinite value of $(\partial f/\partial\varphi)_0$. On the other hand, when $\varphi_0 \to \pi$, $\tan(\varphi_0/2) \sim 2/(\pi-\varphi_0) \to \infty$, so that a finite current corresponds to an infinitely small value of $(\partial f/\partial\varphi)_0$. Therefore, near the electrode, when $\varphi \approx \varphi_0$, the term $(\partial f/\partial\varphi)/\tan\varphi$ in Equation (35) varies as I/φ_0^2 when $\varphi_0 \to 0$ so that it tends toward infinity whenever the current is finite. When $\varphi_0 \to \pi$, it varies as I so that it remains finite whenever the current is finite. This is an interesting property since it shows that when $\varphi_0 \to 0$, the term

$(\partial f/\partial\varphi)/\tan\varphi$ in Equation (35) plays an extremely important role near the electrode surface as soon as $\partial^2 f/\partial\varphi^2$ is not an infinite of higher order. Conversely, since $\partial^2 f/\partial\varphi^2$ is necessarily large when $\varphi_0 \to \pi$, because of the constriction of the diffusional space, the term $(\partial f/\partial\varphi)/\tan\varphi$ plays a negligible role in Equation (35) when $\varphi_0 \to \pi$. Thus, two completely different behaviors arise when $\varphi_0 \to 0$ or $\varphi_0 \to \pi$ albeit the electrode radius tends to be infinitely small in both cases since $R_0\sin\varphi_0 = R_0\sin(\pi - \varphi_0)$. This occurs because the diffusional field converges near the electrode surface when $\varphi_0 \to 0$, while it diverges when $\varphi_0 \to \pi$.

Delineation of the different electrochemical kinetic behaviors

Overview of diffusion in a spherical shell: Examination of Figure 1a shows that the diffusional problem depends on the respective magnitude of three scaling lengths: 1) $R_0(\pi - \varphi_0)$, the maximum length available for diffusion on the spherical shell; 2) $R_0\sin\varphi_0$, the radius of the contact disk of the shell with the surface which acts here as the electrode since electrons can only be transferred by the electrode to the shell at its perimeter; 3) the thickness of the diffusion layer for any electrochemical experiment of duration θ. Within the Einstein – Schmoluchowski framework of diffusion that has been shown above to apply to the system at hand, during a time θ, a diffusing particle walks over the distance $(2D_{hop}\theta)^{1/2}$,[1] so that at time θ the extremity of the diffusion layer is located at the angle φ_{dif} given by $R_0(\phi_{dif} - \varphi_0) \approx (2D_{hop}\theta)^{1/2}$.

Since the maximal diffusion length available on the spherical shell is $R_0(\pi - \varphi_0)$, the system may experience a semi-infinite diffusion only when $(2D_{hop}\theta)^{1/2} \ll R_0(\pi - \varphi_0)$. Otherwise, when $(2D_{hop}\theta)^{1/2} \gg R_0(\pi - \varphi_0)$, the diffusion layer reaches the top ($\varphi_{dif} = \pi$) of the spherical shell much before the end of the electrochemical perturbation and all material present on the shell is electrolyzed at time θ, so that the system is expected to behave as a thin layer of adsorbed species.When the system is under semi-infinite diffusion $(2D_{hop}\theta)^{1/2} \ll R_0$ since $(\pi - \varphi_0)$ is at most commensurable to unity (viz., $0 \le (\pi - \varphi_0) \le \pi$). Therefore, the spherical curvature of the shell is negligible under these conditions. The system then behaves as if diffusion was occurring in a plane perpendicular to the axis of symmetry of the shell. Its behavior depends only on the size of the diffusion layer, $(2D_{hop}\theta)^{1/2}$, relative to the radius of the electrode, $R_0\sin\varphi_0$. When $(2D_{hop}\theta)^{1/2} \ll R_0\sin\varphi_0$, the size of the diffusion layer is sufficiently small for the convergence ($\varphi_0 \le \pi/2$) or divergence ($\varphi_0 \ge \pi/2$) of the diffusional field to be negligible, so that the system behaves as if experiencing planar diffusion.[49] In the converse situation, the system must obey quasi-steady state cylindrical diffusion[2, 49] provided it may behave under conditions of semi-infinite diffusion, that is, provided that $R_0\sin\varphi_0 \ll (D_{hop}\theta)^{1/2}$ and $(D_{hop}\theta)^{1/2} \ll R_0(\pi - \varphi_0)$ may be fulfilled simultaneously.When φ_0 is very small compared to π, $R_0(\pi - \varphi_0) \approx R_0\pi$, and $\sin\varphi_0 \to 0$, so that the above double inequality may be verified. Therefore, upon increasing the electrochemical perturbation duration θ, the system shifts from planar diffusion[1] ($(D_{hop}\theta)^{1/2} \ll R_0\sin\varphi_0$) to planar cylindrical diffusion[2, 49, 50] ($R_0\sin\varphi_0 \ll (D_{hop}\theta)^{1/2} \ll \pi R_0$), and then behaves as a thin layer of adsorbed material ($\pi R_0 \ll (D_{hop}\theta)^{1/2}$).[1, 51] When φ_0 is not very small compared to π, one has either $R_0\sin\varphi_0$ commensurable to R_0 (that is, when φ_0 differs significantly from π) or $R_0(\pi - \varphi_0) \approx R_0\sin\varphi_0$ (that is, when $\varphi_0 \approx \pi$, since $(\pi - \varphi_0) \approx \sin(\pi - \varphi_0) = \sin\varphi_0$). Therefore, the above double inequality cannot be fulfilled since $R_0\sin\varphi_0$ and $R_0(\pi - \varphi_0)$ are commensurable. This means that the quasi-steady state cylindrical behavior cannot be observed. In other words, upon increasing the electrochemical perturbation duration θ, the system shifts directly from a planar diffusion regime ($(D_{hop}\theta)^{1/2} \ll R_0\sin\varphi_0$) to a situation where it behaves as a thin film of adsorbed material ($R_0(\pi - \varphi_0) \approx R_0\sin\varphi_0 \ll (D_{hop}\theta)^{1/2}$). This simple analysis demonstrates that the magnitude of $(D_{hop}\theta)^{1/2}$, the length of the diffusion layer, vis a vis the system's two characteristic lengths, $R_0\sin\varphi_0$ and $R_0(\pi - \varphi_0)$, is crucial. Furthermore, it shows the great complexity of this diffusional problem which depends not only on the respective magnitude of the three lengths mentioned above, but also on φ_0. In particular, this intuitive analysis predicts the possible occurrence of a quasi-steady state diffusional regime only when φ_0 is very small. This is to be related to the observation made above on the respective magnitude of $\partial^2 f/\partial\varphi^2$ and $(\partial f/\partial\varphi)/\tan\varphi$ when φ_0 is small enough.

Analysis of the diffusion problem: Equation (35) governs the occurrence of any of the three different diffusion regimes that may occur as a function of the time scale of the electrochemical experiments. To delineate these three different regimes more precisely than above let us introduce the dimensionless variables in Equations (38) and (39), where θ is the duration of the electrochemical experiment.

$$\text{time:} \qquad \tau = t/\theta \tag{38}$$

$$\text{space:}^{[2, 49, 50]} \qquad \eta = [2R_0\tan(\varphi_0/2)/(D_{hop}\theta)^{1/2}]\ \ln[\tan(\varphi/2)/\tan(\varphi_0/2)] \tag{39}$$

With these variables, the time τ is unity at the moment of measurement and the space η varies between zero and infinity when the diffusion layer describes the whole spherical shell, that is from φ_0 to π. This allows Equation (35) to be rewritten as in Equation (40) (note that $\partial\eta/\partial\varphi = [2R_0\tan(\varphi_0/2)/(D_{hop}\theta)^{1/2}]/\sin\varphi$, and that $\sin\varphi = 2\tan(\varphi/2)/[1 + \tan^2(\varphi/2)]$) where D^* plays the role of a space dependent diffusion coefficient [Eq. (41)].[2, 49, 50]

$$\partial f/\partial\tau = D^*\partial^2 f/\partial\eta^2 \tag{40}$$

$$D^* = \{\tan(\varphi_0/2)[1 + \tan^2(\varphi/2)]/\tan(\varphi/2)\}^2 \tag{41}$$

Thus inserting Equation (39) in Equation (41) gives Equation (42), where β is given by Equation (43).

$$D^* = \exp(-\beta\eta)[1 + \tan^2(\varphi_0/2)\exp(\beta\eta)]^2 \tag{42}$$

$$\beta = (D_{hop}\theta)^{1/2}/[R_0\tan(\varphi_0/2)] \tag{43}$$

The formulation in Equation (40) shows immediately that the problem is identical to that of planar diffusion provided that D^* is constant.[1] Equation (41) shows that this may happen only when $\varphi \approx \varphi_0$ over the whole diffusion layer

© WILEY-VCH Verlag GmbH, D-69451 Weinheim, 2001
0947-6539/01/0710-2212 $ 17.50+.50/0 *Chem. Eur. J.* **2001**, *7*, No. 10

thickness. Indeed, under such conditions, $D^* \approx [1 + \tan^2(\varphi_0/2)]^2$, so that Equation (44) is valid where $\eta^* = \eta/[1 + \tan^2(\varphi_0/2)]$.

$$\partial f/\partial \tau \approx \partial^2 f/\partial \eta^{*2} \quad (44)$$

From Equation (42), this requires that $\beta\eta \to 0$. In planar diffusion the diffusion layer length is $\eta^*_{dif} \approx 1$ at $\tau = 1$. It follows that $\beta\eta_{dif} \approx \beta[1 + \tan^2(\varphi_0/2)]$, so that taking Equation (43) into account shows that $\beta\eta_{dif} \to 0$ is equivalent to $[(D_{hop}\theta)^{1/2}/R_0] \ll \sin\varphi_0$. If $\beta\eta_{dif} \to \infty$, that is, when $R_0\sin\varphi_0 \ll (D_{hop}\theta)^{1/2}$, two cases may arise depending on the size of φ_0. When φ_0 is infinitely small, the bracketed term in Equation (42) may tend towards unity even if $\beta\eta \to \infty$. This occurs provided that Equation (45) is valid.

$$\beta\eta_{diff} \ll -\ 2\ln[\tan(\varphi_0/2)] \approx -\ln(\sin\varphi_0) \quad (45)$$

When this is the case, Equation (40) can be rewritten as Equation (46) and characterizes a cylindrical planar diffusion,[2, 49, 50] that is, occurring within a plane perpendicular to the axis of the cylindrical electrode.

$$\partial f/\partial \tau \approx \exp(-\beta\eta)\partial^2 f/\partial \eta^2 \quad (46)$$

Under such conditions, the maximal extension of the diffusion layer is given by Equation (47).[2, 49]

$$\eta_{dif} \approx 2(\ln\beta)/\beta \quad (47)$$

This situation may then occur only when $R_0\sin\varphi_0 \ll (D_{hop}\theta)^{1/2} \ll R_0$. In other words, when $(D_{hop}\theta)^{1/2}$ is sufficiently large for the diffusion process to experience the cylindrical curvature of the space around the electrode (whose radius is $R_0\sin\varphi_0 \ll R_0$) but sufficiently small for the curvature of the spherical shell (of radius R_0) to be neglected. As explained above, this situation may occur only when φ_0 is infinitely small, since when φ_0 is finite, the above double inequality is impossible to fulfill, so Equation (46) cannot apply anymore.

D^* is infinite whenever $(D_{hop}\theta)^{1/2}/R_0\sin\varphi_0 \to \infty$ (φ_0 finite, vide supra or $(D_{hop}\theta)^{1/2}/R_0 \to \infty$ (φ_0 infinitely small). Indeed, in both cases, Equation (42) can then be rewritten as Equation (48).

$$D^* \approx \exp(\beta\eta)\tan^4(\varphi_0/2) \to \infty \quad (48)$$

To investigate this regime, it is important to note that $\partial f/\partial \tau$ in Equation (40) must remain finite except at possible discontinuities of the electrochemical perturbation, therefore, when $D^* \to \infty$ Eqation (49) becomes valid.

$$\partial^2 f/\partial \eta^2 \to 0 \quad (49)$$

This establishes that the system obeys the steady state. It follows that $\partial f/\partial \eta \approx$ constant, so that $f \to f_0 + (\partial f/\partial \eta)_0\eta$, where the subscript indicates that the value is taken at $\eta = 0$, that is, at $\varphi = \varphi_0$. Since by construction $f \leq 1$, this implies that $(\partial f/\partial \eta)_0 \leq (1 - f_0)/\eta_{dif}$. Owing to the definition of η in Equation (39), $\eta \to \infty$ when $\varphi \to \pi$. When the diffusion layer extends over the whole spherical shell (that is, when $\eta_{dif} \to \infty$) one has necessarily $(\partial f/\partial \eta)_0 \to 0$. This implies that $f \approx f_0$ over most of the shell. Let us then introduce the dimensionless potential [Eq. (50)], where E is the electrode potential and E^0 is the formal potential of the A/B redox couple.

$$\xi = nF(E^0 - E)/RT \quad (50)$$

For a Nernstian (viz., a fast an reversible) electron transfer, for example, one has then $f_0 = [1 + \exp(\xi)]^{-1}$. To evaluate the current, Equation (37) is no longer useful; indeed, since $(\partial f/\partial \eta)_0 \to 0$, that is, $(\partial f/\partial \varphi)_0 \to 0$, it amounts only to expressing that the current is considerably smaller than in the limiting situations identified above. However, since $f \approx f_0 = [1 + \exp(\xi)]^{-1}$ over most of the shell, the current may be obtained from the elementary charge $dq = I\mathrm{d}t$ consumed during an elementary time dt. This elementary charge is equivalent to consuming $\mathrm{d}N = -N_0(\mathrm{d}f/\mathrm{d}t)\mathrm{d}t$ sites A, so that $I = -\mathrm{d}q/\mathrm{d}t = ne(\mathrm{d}N/\mathrm{d}t) \approx neN_0(\mathrm{d}f_0/\mathrm{d}\xi)(\mathrm{d}\xi/\mathrm{d}t)$, and therefore Equation (51) is valid.

$$I = -neN_0\{\exp(\xi)/[(1 + \exp(\xi)]^2\}(\mathrm{d}\xi/\mathrm{d}t) \quad (51)$$

The expression in Equation (51) is identical to that obtained under the same conditions for any film of electroactive material of thickness l deposited on an electrode when $(D\theta)^{1/2} \gg l$, where D is the diffusion coefficient (or the apparent diffusion coefficient) within the film. In other words, the exact geometry of the space in which diffusion occurs is irrelevant.[1, 51] Therefore, we do not need to pursue the solution of this problem when the system is not Nernstian, since it is already well established.

To conclude this section, let us express the current in the general case (for any β and φ_0) based on the present dimensionless variables. With these notations, the current [Eq. (37)] can be expressed by Equation (52), where Ψ [Eq. (53)] is the dimensionless current.

$$I = -[2\tan(\varphi_0/2)/(1 + \cos\varphi_0)](neN_0/\theta)(D_{hop}\theta/R_0^2)^{1/2}\Psi \quad (52)$$

$$\Psi = (\partial f/\partial \eta)_0 \quad (53)$$

This allows the formulation of the dimensionless current in the three limiting cases [Eqs. (54) – (56)] that have been identified above as a function of β and φ_0 values (the expressions are given for a Nernstian electron transfer at the electrode surface; vide infra for slower charge transfer cases).

Case I

$[(D_{hop}\theta)^{1/2}/R_0\sin\varphi_0 \to 0,\ 0 \leq \varphi_0 \leq \pi;$ Eq. (44)] (*planar diffusion*):[1]

$$\Psi_I = (\partial f/\partial \eta^*)_0[(1 + \cos\varphi_0)/2] \quad (54)$$

Case II

$[(D_{hop}\theta)^{1/2}/R_0\sin\varphi_0 \to \infty$ and $(D_{hop}\theta)^{1/2}/R_0 \to 0,\ 0 \leq \varphi_0 \leq \pi/2;$ Eq. (46)] (*cylindrical diffusion*):[2, 49, 50]

$$\Psi_{II} = [\beta/(2\ln\beta)]/[1 + \exp(-\xi)] \quad (55)$$

Case III

$[(D_{hop}\theta)^{1/2}/R_0 \rightarrow \infty$, when $0 \leq \varphi_0 \leq \pi/2$, or $(D_{hop}\theta)^{1/2}/R_0 \sin\varphi_0 \rightarrow \infty$, when $\pi/2 \leq \varphi_0 \leq \pi$; Eq. (51)] (*adsorption*):[1, 51]

$$\Psi_{III} = [R_0/(D_{hop}\theta)^{1/2}][(1+\cos\varphi_0)^2/2\sin\varphi_0]\{\exp(\xi)/[(1+\exp(\xi)]^2\}(d\xi/d\tau) \quad (56)$$

In Equation (54) $(\partial f/\partial\eta^*)_0$ is a constant that depends on the electrochemical perturbation but that is independent of N_0, β, or φ_0. For example, in cyclic voltammetry $(\partial f/\partial\eta^*)_0 = 0.446\varepsilon$ at the peak currents for a Nernstian electron wave ($\varepsilon = 1$ for the forward wave, and $\varepsilon = -1$ for the backward wave when the scan inversion is performed sufficiently far after the forward peak).

The existence of these three different cases is controlled by Equation (35) so that they are not related to a specific electrochemical method or controlled by the kinetics of electron transfer at the electrode surface. However, the exact electrochemical behavior observed necessarily depends on the method and on the kinetics of electron transfer at the electrode surface, owing to the terms $(\partial f/\partial\eta^*)_0$ in Equation (54) or $(d\xi/d\tau)$ in Equation (56) (note that in this respect the term $\exp(\xi)/[(1+\exp(\xi)]^2$ in Equation (56) is valid only for a Nernstian electron transfer; vide infra for a non Nernstian case). The electrochemical behavior observed in case II corresponds to a quasi-steady state behavior, so it is independent of the electrochemical method,[2, 49, 50] the current being solely a function of the electrode potential and of the kinetics of electron transfer at the electrode surface (similarly the term $1/[1+\exp(\xi)]$ in Equation (55) is valid only for a Nernstian electron transfer; vide infra for a non Nernstian case).

Each limiting case predominates over the two others within specific domains of the (β,φ_0) space. However, β is a function of φ_0 which describes the geometric shape of the shell, and of $D_{hop}\theta/R_0^2$ which describes the electrochemical time scale (θ) relative to the duration of diffusion over the whole shell (D_{hop}/R_0^2). For experimental purposes, it is more convenient to separate the two effects. This is easily performed by defining β^* according to Equation (57) so that it is independent of φ_0.

$$\beta^* = [\beta\tan(\varphi_0/2)]^2 = D_{hop}\theta/R_0^2 \quad (57)$$

Schematic domains of predominance of each limiting case I – III, may be indicated through a zone diagram in the (β^*,φ_0) space (Figure 3a). In this schematic diagram, the boundaries between two limiting cases have been set arbitrarily so as to correspond to $\beta^* = 1$ and or $\beta^*\sin^2\varphi_0 = 1$, respectively. In practice each boundary has a given thickness corresponding to the progressive transition between the two limiting cases (compare Figures 3b, c). This diagram suggests that a pure case II cannot be observed unless φ_0 achieves extremely small values. In practice, when φ_0 is very small, one site occupies an average cone angle $\Omega_{site} = 4\pi/N_0$, which corresponds to a disk delimited by the angle $\varphi_{site} = \arccos(1 - \Omega_{site}/2\pi)$ on the spherical shell, that is, to $\delta\varphi_{site} \approx 2/N_0^{1/2}$ within better than 3% provided that N_0 is larger than 10. Thus, if the dendrimer retains a spherical shape when it rests on the electrode surface, the minimal angle φ_0 with physical relevance in our model is given by Equation (58).

$$(\varphi_0)_{min} \approx \delta\varphi_{site} = 4/N_0^{1/2} \quad (58)$$

For $N_0 = 64$, this gives $(\varphi_0)_{min}/\pi \approx 0.15$. The maximum value of φ_0 depends on the compactability of the chains that link each redox site to the center of the dendrimer. However it is intuitive that $(\varphi_0)_{max}$ cannot approach π without introducing

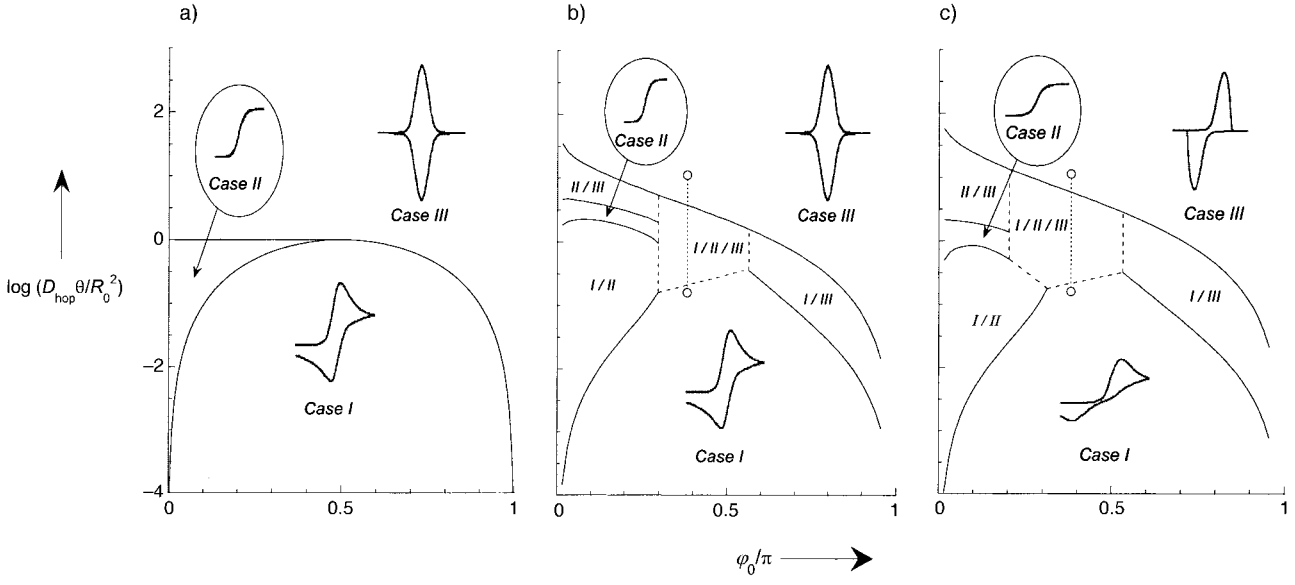

Figure 3. Kinetic zone diagrams corresponding to the three different diffusional behaviors observed as a function of $\beta^* = D_{hop}\theta/R_0^2$ and φ_0. a) Schematic zone diagram. b) Zone diagram computed for cyclic voltammetry ($\theta = RT/nFv$) for a Nernstian electron transfer at the electrode surface. The limits between each case and their transitions are drawn considering a 10% precision on the current intensity of the voltammetric peak. c) Same as b) but for a totally irreversible heterogeneous charge transfer. See Table 1 for the voltammetric peak characteristics in each pure mechanistic zone. In b) and c) the vertical dotted segment indicates the projection of the path followed by the system when the scan rate is increased from 0.036 MV s^{-1} (top circle) to 2.52 MV s^{-1} (bottom circle).

© WILEY-VCH Verlag GmbH, D-69451 Weinheim, 2001
0947-6539/01/0710-2214 $ 17.50+.50/0 *Chem. Eur. J.* **2001**, *7*, No. 10

severe strains on the linkers. Therefore, in the zone diagram of Figure 3a, the outer domains around $\varphi_0/\pi \approx 0$ or 1 have no experimental significance. This shows that in any experimentally realistic situation, a pure case II will be difficult to observe, although it may still play a significant role by contaminating the two others cases and their transition as soon as φ_0 is less than about $\pi/2$.

Effect of charge transfer kinetics at the electrode surface: In the previous section we have considered a Nernstian electron transfer in order to delineate the intricacies of the diffusional problem at hand. However, for nanometric dendrimers and average D_{hop} values, Figure 3a, shows that the observation of a transition from case III to case I requires extremely short time scales. For example for $D_{hop} = 5 \times 10^{-6}$ cm^{2}s^{-1} (vide infra) and $R_0 = 10$ nm, the maximum time θ_{max} allowed for observing such a transition, such as $D_{hop}\theta_{max}/R_0^2 = 1$ (Figure 3a), is of the order of 100 ns, a number which corresponds to a scan rate in the range of a few tenths of a megavolt per second. Furthermore, even for reasonably small φ_0 values, $R_0 \sin\varphi_0$, the radius of the disk through which electrical contact between the electrode and the redox spherical shell is made, is extremely small. Since the edge of this disk acts as the electrode for the spherical shell, extremely large rate constants of electrode transfer are required to allow Nernstian behavior.[2, 49] So, even if the Nernstian approximation is extremely useful in delineating the different kinetic situations that may occur, it is unlikely to be easily fulfilled experimentally for nanometric dendrimers and small φ_0 angles. It is necessary to consider the effects of the kinetics of heterogeneous electron transfer at the edge of the disk on which the spherical shell rests.

Considering Butler–Volmer kinetics[1] and denoting $k^{el} = k_S \exp(\alpha\xi)$ the electron transfer rate constant (α being the electron transfer coefficient and k_S the rate constant at $E = E^0$) one obtains Equation (59) where C_A and C_B are expressed in molecules *per* unit of volume.

$$I = -ne(2\pi R_0 d \sin\varphi_0) k_S \exp(\alpha\xi)[C_A - C_B \exp(-\xi)]_0 \quad (59)$$

Introducing the dimensionless variables in Equations (39) and (53) and equating to the expressions in Equations (37) and (59) gives Equation (60), where Λ [Eq. (61)] is the dimensionless rate of electron transfer.

$$f_0 = [1 + \exp(\xi)]^{-1} + (\Psi/\Lambda)\{\exp(-\alpha\xi)/[1 + \exp(-\xi)]\} \quad (60)$$

$$\Lambda = k_S[(1 + \cos\varphi_0)/2](\theta/D_{hop})^{1/2} \quad (61)$$

Note that Λ, as defined in Equation (61) mixes intrinsic components of the system at hand (k_S, R_0, φ_0, D_{hop}) with θ which characterizes the time scale of the electrochemical method and which is already incorporated into the dimensionless parameter β^* [Eq. (57)]. From an experimental point of view, it is more advisable to separate the intrinsic components from the time scale of the experiment by introducing $\Lambda^* = (k_S R_0/D_{hop})(1 + \cos\varphi_0)/2$, so that Equation (61) becomes $\Lambda = \Lambda^* \beta^{*1/2}$. Λ^* characterizes just the intrinsic heterogeneous kinetic properties independently of the time scale of the electrochemical perturbation, and is thus constant when θ varies. With these notations, the kinetic behavior of the system is regulated by three independent dimensionless parameters, φ_0, which characterizes only its geometry, Λ^*, which characterizes the intrinsic charge transfer kinetics at the electrode surface, and β^*, which characterizes the rate of electron hopping and the time scale of the electrochemical perturbation. The experimental interest of this new triplet of dimensionless parameters is that only β^* varies with the scan rate for a given system. However, as above for $\beta = \beta^{*1/2}/\tan(\varphi_0/2)$ [Eq. (57)], Λ results more conveniently from a mathematical point of view, so that we continue hereafter with this parameter.

When Λ is excessively large vis a vis Ψ, the second term in the right-hand side of Equation (60) vanishes and Equation (62) becomes valid showing that system behaves in a Nernstian fashion; the voltammetric waves are observed around $\xi = 0$.

$$f_0 = [1 + \exp(\xi)]^{-1} \quad (62)$$

Conversely, when Λ is excessively small, the rate of electron transfer is too small to afford a significant current in the potential range around E^0, so that the voltammetric peaks are shifted towards large $|\xi|$ values.[1] Then, by denoting $\xi^* = \alpha^*\xi + (\ln\Lambda)$ where $\alpha^* = \alpha$ for the forward wave or $\alpha^* = \alpha - 1$ for the backwards wave, Equation (62) simplifies into Equation (63) for the forward wave and into Equation (64) for the backward wave (note that then Ψ is negative), so that the system follows slow charge transfer kinetics.[1, 52]

$$f_0 = \Psi \exp(-\xi^*) \quad (63)$$

$$f_0 = 1 + \Psi \exp(-\xi^*) \quad (64)$$

In this slow charge transfer limit, the peak currents given above in Equations (54)–(56) for the Nernstian situations become Equations (65)–(67) for cases I–III, respectively.

Case I

$[(D_{hop}\theta)^{1/2}/R_0 \sin\varphi_0 \to 0,\ 0 \le \varphi_0 \le \pi;$ Eq. (44)] (*planar diffusion*):[1]

$$\Psi_I = (\partial f/\partial \eta^*)_0[(1 + \cos\varphi_0)/2] \quad (65)$$

Case II

$[(D_{hop}\theta)^{1/2}/R_0 \sin\varphi_0 \to \infty$ and $(D_{hop}\theta)^{1/2}/R_0 \to 0,\ 0 \le \varphi_0 \le \pi/2;$ Eq. (46)] (*cylindrical diffusion*):[2, 49, 50]

$$\Psi_{II} = [\beta/(2\ln\beta)]/[1 + \exp(-\xi^*)] \quad (66)$$

Case III

$[(D_{hop}\theta)^{1/2}/R_0 \to \infty$, when $0 \le \varphi_0 \le \pi/2$, or $(D_{hop}\theta)^{1/2}/R_0 \sin\varphi_0 \to \infty$, when $\pi/2 \le \varphi_0 \le \pi$; Eq. (51)] (*adsorption*):[1, 51]

$$\Psi_{III} = [R_0/(D_{hop}\theta)^{1/2}][(1 + \cos\varphi_0)/2\tan(\varphi_0/2)]\Xi_\alpha(\xi^*) \quad (67)$$

In Equation (65), $(\partial f/\partial\eta^*)_0$ is a constant that depends on the electrochemical perturbation but that is independent of N_0, β or φ_0. For example, in cyclic voltammetry[52] $(\partial f/\partial\eta^*)_0 = 0.496\varepsilon[\alpha\varepsilon + (1-\varepsilon)/2]^{1/2}$ at the peak currents for a Nernstian electron wave ($\varepsilon = 1$ for the forward wave, and $\varepsilon = -1$ for the backward wave when the scan inversion is performed sufficiently far after the forward peak). Similarly, $\Xi_\alpha(\xi^*)$ in Equation (42) is an analytical function of α and ξ^* that depends on the electrochemical perturbation (vide infra for cyclic voltammetry).

In the intermediate range of Λ values, the general Equation (60) applies without simplification so f_0 is controlled simultaneously by kinetic and thermodynamic factors (quasi reversible charge transfer kinetics). It is therefore understood that the existence of slow charge transfer (vs. a Nernstian system) affects the electrochemical wave shapes and position but does not alter the respective positions of the three limiting cases in the $[(D_{hop}\theta)^{1/2}/R_0, \sin\varphi_0]$ domain. In other words, the schematic picture shown in Figure 3a is conserved. To pursue this analysis, we need now to particularize it to the case of cyclic voltammetry.

Formulation of the voltammetric problem: In voltammetric experiments the electrode potential is scanned linearly with time from a potential E_i where the species of interest is not electroactive ($nF(E_i - E^0) \ll 0$, E^0 being the formal potential of the species, so that $f = 1$ over the whole shell) to a potential E_f located on the current plateau ($nF(E_f - E^0) \gg 0$) of the species for the redox reaction of interest; the potential scan direction is then reversed. Denoting v as the algebraic potential scan rate ($vn > 0$, that is, $v > 0$ for a reduction, since $n > 0$; $v < 0$ for an oxidation, since $n < 0$), $\xi_i = nF(E_i - E^0)$, $\xi_f = nF(E_f - E^0)$ and $t_f = (E_i - E_f)/v$, one obtains with the above defined dimensionless variables Equation (68) for the forward scan ($\tau \le \tau_f = nFvt_f/RT$, that is, $\xi \le \xi_f = nF(E_f - E^0)$) and Equation (69) for the backward scan ($\tau \ge \tau_f$).

$$\xi = \xi_i + (nFv\theta/RT)\tau \tag{68}$$

$$\xi = \xi_i + 2(nFv\theta/RT)\tau_f - (nFv\theta/RT)\tau \tag{69}$$

Equations (68) and (69) show that it is advisable to define θ as given in Equation (70)[52] for cyclic voltammetry.

$$\theta = RT/nFv \tag{70}$$

In this way the Equations (68) and (69) simplify into $\xi = \xi_i + \tau$ and $\xi = \xi_i + 2\tau_f - \tau$, respectively. In the following we assume everywhere that ξ_i is negative enough (that is, $\xi_i \le -10$) for the forward wave to be independent of its exact value. Similarly, ξ_f is assumed positive enough (that is, $\xi_f \ge +10$) for the backward wave to be independent of its exact value.

With those notations, the voltammetric problem amounts to solving the diffusion Equations (40) and (42) with the boundary conditions given in Equations (71) – (73).

$$\xi = \xi_i,\ \eta \ge 0: \quad f = 1 \tag{71}$$

$$\xi > \xi_{in},\ \eta = 0: \quad f_0 = [1 + \exp(\xi)]^{-1} + (\Psi/\Lambda)\{\exp(-\alpha\xi)/[1 + \exp(-\xi)]\} \tag{72}$$

$$\xi > \xi_{in},\ \eta \to \infty: \quad (\partial f/\partial\eta)_\pi \to 0 \tag{73}$$

Owing to Equations (61) and (43) and to the present definition of θ in Equation (70) Λ and β can be defined as given in Equations (74) and (75), respectively.

$$\Lambda = k_S[(1 + \cos\varphi_0)/2](RT/nFvD_{hop})^{1/2} \tag{74}$$

$$\beta = (nFvD_{hop}/RT)^{1/2}/[R_0\tan(\varphi_0/2)] \tag{75}$$

Resolution of this system affords the value of $\Psi = (\partial f/\partial\eta)_0$ as a function of τ, from which the experimental voltammetric current is readily obtained by application of Equation (76) owing to Equations (52) and (70).

$$I = -[2\tan(\varphi_0/2)/(1 + \cos\varphi_0)][neN_0(nFvD_{hop}/RT)^{1/2}/R_0]\Psi \tag{76}$$

In a general case, this system must be solved numerically. However, the above analyses have shown that its solution $\Psi(\tau)$ tends towards known asymptotic values when $(nFvD_{hop}/RT)^{1/2}/R_0$, $(nFvD_{hop}/RT)^{1/2}/(R_0\sin\varphi_0)$ and Λ take extreme values. When $\Lambda \to \infty$ (Nernstian behavior) these limiting solutions are given in Equations (54) – (56) where in cyclic voltammetry $d\xi/d\tau = 1$ for the forward scan and $d\xi/d\tau = -1$ for the backward scan in Equation (56). Similarly, when $\Lambda \to 0$ (slow charge transfer) these limiting solutions are given in Equations (65) – (67) where the function $\Xi_\alpha(\xi^*)$ (case III, Equation (67)) needs to be established.

To obtain the expression of Ψ in case III, we proceed as follows. As established for the derivation of Equation (51), and using Equation (52), within the limiting case III, $\Psi(\xi^*)$ is given by Equation (77), where $\xi^* = \alpha^*\xi + \ln\Lambda$ and $\alpha^* = \alpha$ for the forward scan or $\alpha^* = (\alpha - 1)$ for the backward one, that is, by Equation (78).

$$\Psi = -\ [(1 + \cos\varphi_0)^2/2\sin\varphi_0](nFvR_0^2/D_{hop}RT)^{1/2}[(d\xi^*/d\tau)](df_0/d\xi^*) \tag{77}$$

$$\Psi = -\varepsilon\gamma\alpha^*(df_0/d\xi^*) \tag{78}$$

In Equation (78), $\gamma = [(1 + \cos\varphi_0)^2/2\sin\varphi_0](nFvR_0^2/D_{hop}RT)^{1/2}$, and $\varepsilon = 1$ for the forward scan or $\varepsilon = -1$ for the backward one. Since this situation corresponds to $\Lambda \to 0$, f_0 is given by Equation (63) or (64) for the forward and backward voltammetric scans respectively, that is Equation (79) becomes valid.

$$\Psi/(\varepsilon\gamma\alpha^*) = -\ df_0/d\xi^* = [\Psi - d\Psi/d\xi^*]\exp(-\xi^*) \tag{79}$$

This shows that Ψ is solution of (note that $\Psi \ge 0$ during the forward scan and $\Psi \le 0$ during the backward one) Equation (80) where $\xi^{*\prime} = \xi^* - \ln(\varepsilon\gamma\alpha^*) = \alpha^*\xi + \ln(\Lambda/\varepsilon\gamma\alpha^*)$.

$$d[\ln(\varepsilon\Psi)] = [1 - \exp(\xi^{*\prime})]d\xi^{*\prime} \tag{80}$$

Equation (55) shows that the extrema of Ψ are observed at any ξ value such as $\xi_p^{*\prime} = 0$, viz., at $\xi_p = -\alpha^{-1}\ln(\Lambda/\gamma\alpha)$ for the forward scan, and at $\xi_p = -(1-\alpha)^{-1}\ln[\Lambda/\gamma(1-\alpha)]$ for the backward scan. Integration of Equation (80) affords Equation (81) where 'Y' is an integration constant.

$$\Psi = \varepsilon\exp[\xi^{*\prime} - \exp(\xi^{*\prime})]Y \tag{81}$$

© WILEY-VCH Verlag GmbH, D-69451 Weinheim, 2001
0947-6539/01/0710-2216 $ 17.50+.50/0 *Chem. Eur. J.* **2001**, *7*, No. 10

To evaluate this constant, it is noted that with the present notations, at any potential Equations (63) and (64) afford Equation (82).

$$\Psi = \gamma\alpha^*[(1-\varepsilon)/2 + \varepsilon f_0]\exp(\xi^{*\prime}) \quad (82)$$

$[(1-\varepsilon)/2 + \varepsilon f_0] \to 1$ when $\xi^{*\prime} \to -\infty$, so that, Equation (82) shows that $\Psi \sim \gamma\alpha^*\exp(\xi^{*\prime})$ when $\xi^{*\prime} \to -\infty$. On the other hand, from Equation (81), $\Psi \sim \Upsilon\varepsilon\exp(\xi^{*\prime})$ when $\xi^{*\prime} \to -\infty$, so that $\Upsilon = \varepsilon\gamma\alpha^*$, and Ψ can be given by Equation (83).

$$\Psi = \gamma\alpha^*\exp[\xi^{*\prime} - \exp(\xi^{*\prime})] \quad (83)$$

Equation (57) shows that when $\Lambda \to 0$ (slow charge transfer), the limiting voltammograms observed in case III, are composed of two distorted bell-shaped curves, whose peak currents located at $\xi^{*\prime} = 0$, have the intensity $\gamma\alpha^*/e_N \approx 0.368\gamma\alpha^*$, where e is the Neperian logarithm base, viz., $\ln e_N = 1$. We thus obtain Equations (84) and (85) for the forward wave and Equations (86) and (87) for the backward wave finally for the case III in the slow charge transfer regime.

$$\Psi_{III}^{p} = (\alpha/e_N)[R_0/(D_{hop}\theta)^{1/2}] \times [(1 + \cos\varphi_0)^2/2\sin\varphi_0] \quad (84)$$

$$\xi_{III}^{p} = -\alpha^{-1}\ln[(k_S\theta/\alpha R_0)\tan(\varphi_0/2)] \quad (85)$$

$$\Psi_{III}^{p} = -[(1-\alpha)/e_N][R_0/(D_{hop}\theta)^{1/2}] \cdot [(1+\cos\varphi_0)^2/2\sin\varphi_0] \quad (86)$$

$$\xi_{III}^{p} = (1-\alpha)^{-1}\ln\{[k_S\theta/(1-\alpha)R_0]\tan(\varphi_0/2)\} \quad (87)$$

Again both set of values are identical to those obtained for a thin film of adsorbed electroactive material in the slow charge transfer kinetic regime.[1, 51]

This analysis has identified six different limiting voltammetric regimes and produced the characteristics of the voltammograms obtained in each regime achieved whenever the three key parameters $(nFvD_{hop}/RT)^{1/2}/R_0$, $(nFvD_{hop}/RT)^{1/2}/(R_0\sin\varphi_0)$ and Λ obey the conditions which have been defined in the analysis of each limiting case I, II, and III. When these relationships are not obeyed, analytical expressions cannot be obtained for the peak current and potential values.

However, the numerical solution of the diffusion Equations (40) and (42) associated with the boundary conditions in Equations (71)–(73) allows the prediction of voltammograms for any value of β and Λ [Eqs. (49) and (50)] at any value of φ_0, as well as allowing one to eventually decide how far the system lies from any one of its limiting situations. This was performed (see Experimental Section) in particular to establish the zone diagrams in Figures 3b, c, and all the working curves used in the following discussion. In Figures 3b, c each limiting domain is limited by boundaries that have been arbitrarily set so that the voltammetric current peak intensities deviate by less than 10% from the prediction for the limiting case considered. In particular, those two zone diagrams confirm that a clean case II cannot be observed experimentally except if φ_0 is unrealistically small.

Experimental Results

The electrochemistry of a single layer of adsorbed dendrimers[6–8] was performed at extremely high scan rates by taking advantage of our recent potentiostat design.[3, 4] This design allows performance in the megavolt per second range of scan rates with electronic compensation of the cell resistance so that the voltammograms are undistorted under 2 MVs^{-1}. Figure 4 represents an illustrative series of voltammograms

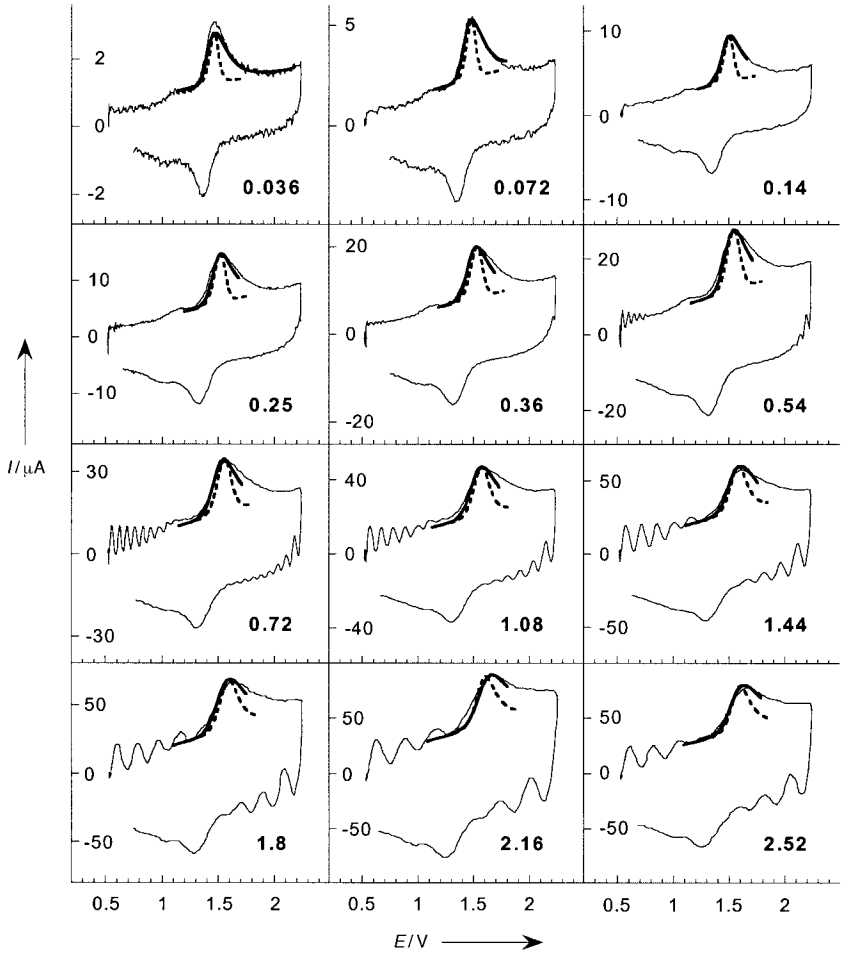

Figure 4. Representative set of the voltammograms of a saturated solution of the dend-64-[$Ru^{II}/Ru^{III}(tpy)_2$] dendrimer (Scheme 1) investigated in this study as a function of the scan rate (number indicated in MVs^{-1} in the bottom right angle of each panel). Voltammetry was performed at room temperature (20 °C) in acetonitrile, 0.6 M NEt_4BF_4, at a platinum disk electrode ($r_0 = 5.0 \pm 0.5$ μm radius). Potentials are given with respect to the platinum pseudo-reference electrode used in this study. Thin curves: experimental voltammograms. Thick dashed curves: predicted anodic voltammetric peaks upon considering a mono-disperse population of dendrimers ($g_0 = 1.6$ and $G(g) = \delta(g - 1.6)$ where δ is the Dirac function). Thick solid curves: predicted anodic voltammetric peaks upon considering the distribution $G(g)$ shown as a solid curve in Figure 7b.

obtained for the dend-64-[Ru(tpy)$_2$] dendrimer investigated in this study (Scheme 1)[6–8] over the megavolt per second range of scan rates. As apparent in these voltammograms, the Faradaic current adds to the capacitive one (which varies as v), yet it remains a large component of the voltammogram owing to the large surfacic concentration of dendrimer. In the low MV s^{-1} range, the Faradaic current response is close to a bell-shape, in agreement with what is expected for a fully oxidized layer of adsorbed species.[1, 51] However, when the scan rate is increased to several MV s^{-1} one observes the development of voltammograms with the expected shape for transient infinite diffusion.[1, 4]

Such data could be obtained only when the electrode was pulsed between sufficiently positive and negative potentials in the presence of the dendrimer before the series of voltammograms were recorded. When this electrochemical *pre*-treatment which forced continuous adsortion/desorption of the dendrimer molecules was not applied, the general pattern shown in Figure 4 was retained, yet the anodic and cathodic peaks were considerably broader, and one could often observe a split of the voltammetric peaks as soon as the scan rate was increased. However, the above pretreatment allowed us to obtain reproducible narrow peaks such as those shown in Figure 4.

Figure 5 presents the variations of the current function $I_p v^{-1/2}$ as a function of the scan rate. In agreement with the observed voltammetric shapes, at the smaller scan rates the current function tends to vary as $v^{1/2}$, reflecting that I_p tends to be proportional to v as required[1, 51] for complete electrolysis of an adsorbed layer (case III, Table 1). For the larger scan rates $I_p v^{-1/2}$ asymptotically approaches a constant plateau, where it tends to be proportional to $v^{1/2}$ as required for a semi-

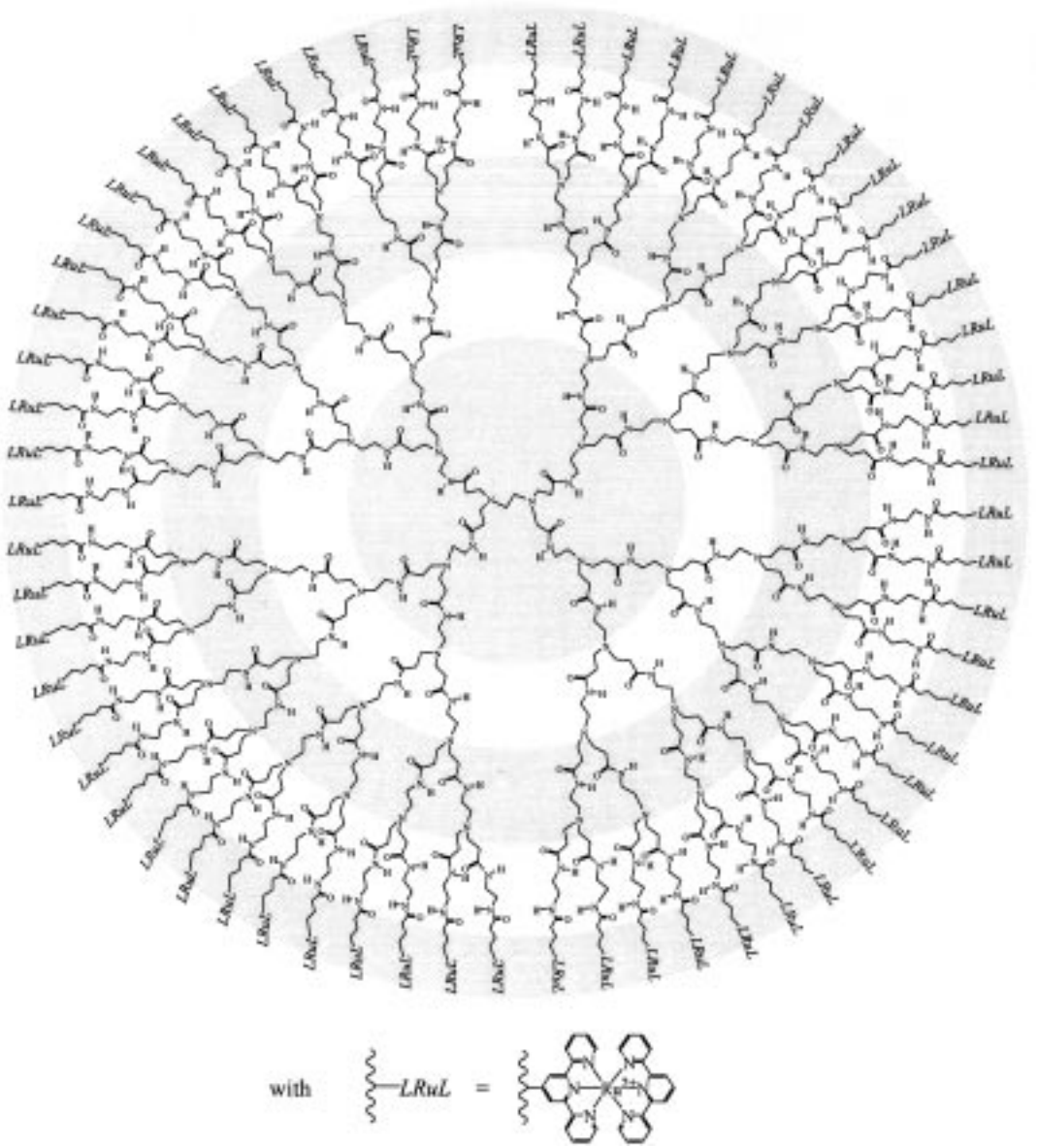

Scheme 1. Structure of fourth generation PAMAM dendrimer with 64 pendant ruthenium terpyridyl moieties (Dend-64-[Ru(tpy)$_2$]). The four central concentric shaded areas represent each generation of the dendritic structure. The external fifth shaded area represents the location of the 64 [Ru(tpy)$_2$] redox centers.

© WILEY-VCH Verlag GmbH, D-69451 Weinheim, 2001
0947-6539/01/0710-2218 $ 17.50+.50/0 *Chem. Eur. J.* **2001**, *7*, No. 10

Table 1. Summary of the different voltammetric characteristics observed for each of the six limiting kinetic situations identified in this study.[a,b]

	Nernstian ($\Lambda \gg 1$)[c]	Slow charge transfer ($\Lambda \ll 1$)[c]
Case I	$I_p/(neN_0) = 0.446 \times (D_{hop}/R_0^2\theta)^{1/2}\tan(\varphi_0/2)$ $E_p = E^0 - 1.09 \times (RT/nF)$[d] $\Delta E_p = 2.18(RT/nF)$[d]	$I_p/(neN_0) = 0.496(\alpha^* D_{hop}/R_0^2\theta)^{1/2}\tan(\varphi_0/2)$ $E_p = E^0 - (RT/\alpha^* nF)[0.780 - \ln(\Lambda\alpha^{*1/2})]$[e] $\Delta E_p = (RT/nF)(0.780 - \ln\Lambda)/[\alpha(1-\alpha)] - (RT/2nF)[\alpha^{-1}\ln\alpha + (1-\alpha)^{-1}\ln(1-\alpha)]$[d]
Case II[e]	$I_p/(neN_0) = (D_{hop}/R_0^2)/(1+\cos\varphi_0)\ln\{D_{hop}\theta/[R_0\tan(\varphi_0/2)]^2\}$ $E_{1/2} = E^0$[d]	$I_p/(neN_0) = (D_{hop}/R_0^2)/(1+\cos\varphi_0)\ln\{D_{hop}\theta/[R_0\tan(\varphi_0/2)]^2\}$ $E_{1/2} = E^0 - (RT/\alpha^* nF)\ln\Lambda$[d]
Case III	$I_p/(neN_0) = 1/(4\theta)$ $E_p = E^0$[d] $\Delta E_p = 0$[d]	$I_p/(neN_0) = \alpha^*/(e_N\theta) \approx 0.368(\alpha^*/\theta)$ $E_p = E^0 - (RT/\alpha^* nF)\ln[(k_S\theta/R_0)\tan(\varphi_0/2)]$[d] $\Delta E_p = -(RT/nF)\ln[(k_S\theta/R_0)\tan(\varphi_0/2)]/[\alpha(1-\alpha)]$[d]

[a] See text and Figure 3 for the kinetic domain of each case I–III as a function of $D_{hop}\theta/R_0^2$ and φ_0. [b] The peak currents are given for one dendrimer molecule; for $N_d = \pi r_0^2 \Gamma_d N_A$ identical dendrimers adsorbed on the electrode surface (N_A being the Avogadro number and Γ_d expressed in moles per unit of surface), the overall experimental current is N_d times that indicated. E_p is the peak potential of the forward wave, and ΔE_p the peak-to-peak potential separation. [c] $\Lambda = k_S(\theta/D_{hop})^{1/2}[(1+\cos\varphi_0)/2]$, $\theta = RT/nFv$ in cyclic voltammetry; α^* represents α when $n > 0$, or $(1-\alpha)$ when $n < 0$. [d] These expressions are given for the case where the reduced and oxidized forms of the dendrimer have the same adsorption isotherms. [e] In case II, a single voltammetric sigmoid wave is observed, so its half wave potential $E_{1/2}$ is indicated.

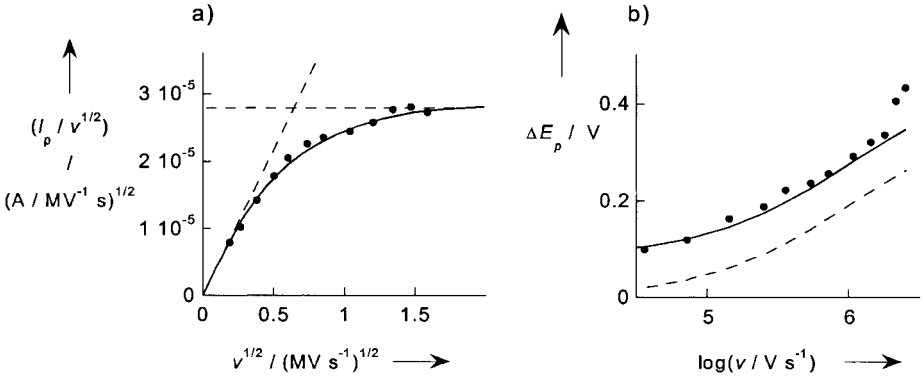

Figure 5. a) Symbols: variations of the anodic peak current intensity $I_p/v^{1/2}$ as a function of the scan rate $v^{1/2}$. Solid curve: predicted variations for $\varphi_0 = 1.2$ rd, $(D_{hop}^{1/2}/R_0) = 4.2 \times 10^3\,s^{-1/2}$, and $(k_S/D_{hop}^{1/2}) = 1.2 \times 10^3\,s^{-1/2}$; horizontal dashed line: high scan rate limit ($I_p/v^{1/2} = 2.81 \times 10^{-5}\,AMV^{-1/2}s^{1/2}$); slanted dashed line: low scan rate limit ($I_p/v = 4.35 \times 10^{-5}\,AMV^{-1}s$). b) Symbols: variations of the peak-to-peak potential difference ΔE_p as a function of the scan rate v. Dashed curve: predicted variations ΔE_p^{th} for $\varphi_0 = 1.2$ rd, $(D_{hop}^{1/2}/R_0) = 4.2 \times 10^3\,s^{-1/2}$, and $(k_S/D_{hop}^{1/2}) = 1.2 \times 10^3\,s^{-1/2}$. Solid curve: $\Delta E_p^{th} + 80$ mV (see text).

infinite diffusion (case I, Table 1). The variations of the peak-to-peak separation, ΔE_p, also agree with this general pattern. Indeed, except for the two highest scan rates where the measurements are contaminated by ohmic drop and filtered by the potentiostat, at sufficiently high scan rates ($v > 0.1\,MV\,s^{-1}$) ΔE_p varies with a slope of 120 ± 10 mV per unit of log(v), which is clear evidence of semi-infinite diffusion (case I) with slow charge transfer kinetics[52] (see Table 1). From this slope, it is deduced that $\alpha = 0.5$ (Table 1).[52] However, at slower scan rates, ΔE_p tends towards a constant value of 80 ± 5 mV. One does not observe a slope close to 240 mV *per* unit of log(v), as expected for case III in the slow charge transfer regime (Table 1).[1, 51] This indicates that the rate of electron transfer at the electrode surface is sufficiently large to yield closely Nernstian behavior in the range where case III is applicable. However, the theoretical results in Table 1 predict that ΔE_p should tend towards zero and not towards a constant value. In fact, the same constant value (80 ± 5 mV) has already been observed at considerably smaller scan rates than those used here ($v < 0.1\,V\,s^{-1}$).[6] Therefore any relationship between this constant ΔE_p limit and any kinetic process is clearly ruled out. We will examine the origin of this term in a later stage of the following discussion.

Discussion

The above results qualitatively follow the main trends elaborated in the previous theory. The only qualitative discrepancy being related to the limit of ΔE_p at small scan rates that is not zero as predicted in the above theory. We will discuss this important point in a second stage of this discussion, since it clearly indicates that upon oxidation/reduction of the ensemble of adsorbed dendrimers, the overall current is not the simple arithmetic multiplication of the electrochemical process occurring at one isolated dendrimer molecule.

Characterization of diffusion within one dendrimer

Analyzing quantitatively the data at hand requires the determination of several experimental parameters (D_{hop}/R_0^2, $k_S/D_{hop}^{1/2}$, and φ_0) which control the values of the dimensionless variables β^* and Λ at a given scan rate. For this we proceed as follows.

As discussed above, the variations of ΔE_p versus log(v) at higher scan rates ($0.1\,MV\,s^{-1} < v < 1.5\,MV\,s^{-1}$) tend towards the asymptotic behavior predicted for case I under slow charge transfer kinetic control. Using the corresponding expression in Table 1, one may deduce the value of $(k_S/D_{hop}^{1/2})[(1+\cos\varphi_0)/2]$. However, at slow scan rates, that is, when the system reaches case III under Nernstian control, $\Delta E_p \approx 80$ mV was determined experimentally instead of the predicted 0 mV. At this stage one does not know whether or not this applies also to the large scan rate range. In other words, one does not know what "zero reference" value to use as the limit for the would-be case I-Nernstian regime ($\Delta E_p = 0$, or 80 mV, or any value in between?) in order to determine $(k_S/D_{hop}^{1/2})[(1+\cos\varphi_0)/2]$.[52] Considering both of these two possible "zero

reference" values, one obtains $5.5 \times 10^2\ s^{-1/2} \leq (k_S/D_{hop}^{1/2})[(1+\cos\varphi_0)/2] \leq 11.5 \times 10^2\ s^{-1/2}$. In the following we retain their average value $(k_S/D_{hop}^{1/2})[(1+\cos\varphi_0)/2] = 8 \times 10^2\ s^{-1/2}$. φ_0 being unknown $k_S/D_{hop}^{1/2}$ cannot be determined yet.

From the limit observed at large scan rates (Figures 5a or 6a one determines that in case I-slow charge transfer regime, $(I_p/A) \rightarrow 2.81 \times 10^{-8}\ (v/V\,s^{-1})^{1/2}$ when $v \rightarrow \infty$. Conversely, when $v \rightarrow 0$, in the case III–Nernstian limit, one has $(I_p/A) \rightarrow 4.35 \times 10^{-11}\ (v/V\,s^{-1})$. From the ratio of these two limits one eliminates the unknown common $N_d e N_0$ factor (Table 1), so that $(D_{hop}/R_0^2)^{1/2}\tan(\varphi_0/2) = 2.9 \times 10^3\ s^{-1/2}$ is calculated when $\alpha = 0.5$. Yet, $k_S/D_{hop}^{1/2}$ and D_{hop}/R_0^2 cannot be determined since φ_0 is still unknown.

This set of relationships gives the required parameters $(D_{hop}/R_0^2,\ k_S/D_{hop}^{1/2})$ as a function of the still unknown φ_0 value: $(D_{hop}/R_0^2)^{1/2} = 2.9 \times 10^3/\tan(\varphi_0/2)$, and $(k_S/D_{hop}^{1/2}) = 8 \times 10^2/[(1+\cos\varphi_0)/2]$, where in each case the constant term is in $s^{-1/2}$. We then performed a series of simulations for a series of constant φ_0 values (Figures 6b, c). As observed in Figures 6b, c, the predicted variations of v/I_p strongly depend on φ_0 over the window of scan rates used in this study even if all curves tend asymptotically towards the same limit (case III–Nernstian) at slow scan rates. This can be easily understood by examination of the zone diagram in Figures 3b or 3c. When φ_0 is extremely small, starting in case III and increasing the scan rate forces the system into the transition zone II/III so as to eventually reach a pure case II; upon increasing further the scan rate, the system is then forced into the transition I/II and finally reaches a pure case I–slow charge transfer. A complete displacement from pure case III to pure case I would then require at least two to three orders of magnitude of scan rates (Figures 3b or 3c). Experimentally one observes such a transition over a slightly less than two orders of magnitude of scan rate (from 0.036 to 2.52 $MV\,s^{-1}$). This clearly shows that φ_0 cannot be small. Whenever φ_0 is larger than about $\pi/2$, the system passes directly from case III to case I upon increasing the scan rate and the corresponding I/III transition requires less than ca. one order of magnitude of scan (Figures 3b or 3c). This shows that φ_0 cannot greatly exceed $\pi/2$. When φ_0 is around $\pi/2$, the transition from case III to case I passes through the general case so that its duration depends critically on φ_0 because this latter controls the amount of interference from the unseen case II (Figures 3b or 3c). As a result, v/I_p variations with v become extremely sensitive to the exact value of φ_0 when it is around $\pi/2$. One may take advantage of this situation to determine φ_0 with an excellent precision. Thus, comparison of the experimental variations of v/I_p as a function of v with the set of working curves presented in Figures 6b, c shows (Figure 6a) that an excellent agreement is observed for $\varphi_0 = 1.2 \pm 0.1\ rd \approx 2\pi/5$. It ensues that $(D_{hop}/R_0^2)^{1/2} = (4.2 \pm 0.5) \times 10^3\ s^{-1/2}$ and that $(k_S/D_{hop}^{1/2}) = (1.2 \pm 0.5) \times 10^3\ s^{-1/2}$.

From the φ_0 value determined above it is deduced that a dendrimer molecule does not rest on the electrode surface by retaining its total spherical solution shape, but that a significant fraction of chain linkers are in close contact with the electrode surface (see Figure 1b). In fact, within the framework of this model, the disk of contact with the electrode has a radius of $R_0\sin\varphi_0 \approx 0.93R_0$. This shows that the adsorbed dendrimer molecule is distorted vis a vis the spherical shape it has in solution,[36–38] and more closely resembles a hemisphere. Assuming that the dendrimer molecule retains its inner volume when it adsorbs on the electrode surface, $R_0 \approx 1.1R_{free}$ where $R_{free} \approx 5$ nm is the estimated radius of a free dendrimer molecule in solution.[6–8] Such data compares extremely well with the result of scanning tunneling microscopy (STM) investigations of related dendrimers on platinum electrode surfaces in which it was noted that the radius of the adsorbed globule was about 10% larger than that calculated for the free molecule.[7]

Using the above R_0 value affords $D_{hop} = 5 \times 10^{-6}\ cm^2 s^{-1}$ and $k_S = 2.5\ cm\,s^{-1}$ based on the above average values of D_{hop}/R_0^2 and $k_S D_{hop}^{-1/2}$. By using Equation (8) and $d = 1.4$ nm for the diameter of one $Ru(tpy)_2$ redox center, the above D_{hop} value gives $k \approx 4.8 \times 10^{-16}\ L\,s^{-1}$. This value corresponds to a would be homogeneous self-exchange rate constant $6kN_A \approx 1.7 \times$

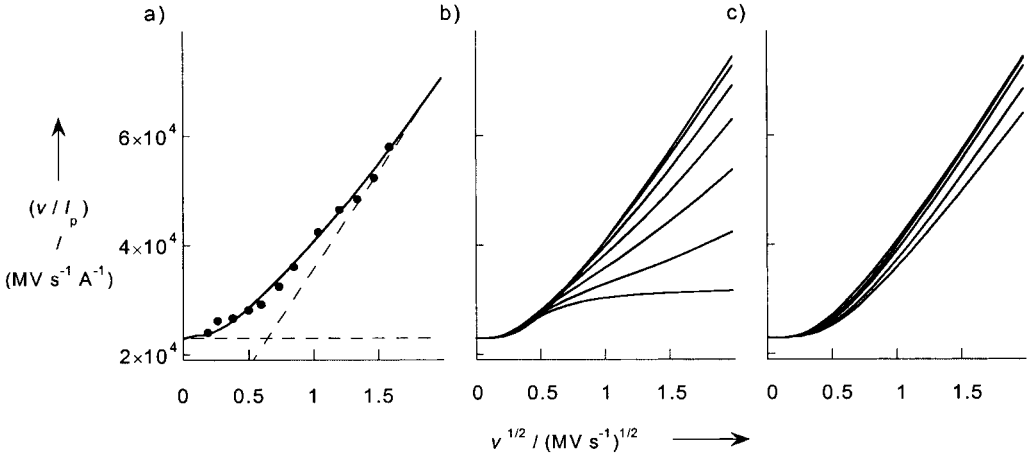

Figure 6. Variations of v/I_p as a function of the scan rate. a) Experimental data (symbols) and predicted variations (solid curve) for $\varphi_0 = 1.2$ rd, $(D_{hop}^{1/2}/R_0) = 4.1 \times 10^3\ s^{-1/2}$, and $(k_S/D_{hop}^{1/2}) = 1.2 \times 10^3\ s^{-1/2}$. Dashed lines: limit at low (horizontal line, $I_p/v = 4.35 \times 10^{-5}\ A\,MV^{-1}s$) or high (slanted line, $I_p/v^{1/2} = 2.81 \times 10^{-5}\ A\,MV^{-1/2}s^{1/2}$) scan rates. b) and c) Predicted behaviors at a series of different φ_0 values for $(D_{hop}^{1/2}/R_0)\tan(\varphi_0/2) = 2.9 \times 10^3\ s^{-1/2}$, and $(k_S/D_{hop}^{1/2})[(1+\cos\varphi_0)/2] = 8 \times 10^2\ s^{-1/2}$; b) from bottom to top, $\varphi_0 = 0.050$, 0.345, 0.640, 0.935, 1.230, 1.525, and 1.820; c) from top to bottom, $\varphi_0 = 1.820$, 2.115, 2.310, 2.610, and 2.900.

© WILEY-VCH Verlag GmbH, D-69451 Weinheim, 2001
0947-6539/01/0710-2220 $ 17.50+.50/0 *Chem. Eur. J.* **2001**, *7*, No. 10

$10^9\,\mathrm{L\,mol\,s^{-1}}$ in solution. Note that such a rate validates a posteriori our initial assumption concerning the negligible role of direct electron tunneling between the electrode surface and the redox sites distributed on the dendrimer outer shell. The above value of $6kN_A \approx 1.7\times10^9\,\mathrm{L\,mol\,s^{-1}}$ ought to be compared to k_{act}^{soln}, the isotopic rate constant of the electron transfer between free $[Ru^{II}/Ru^{III}(tpy)_2]$ redox centers. To the best of our knowledge, k_{act}^{soln} has never been determined for $[Ru^{II}/Ru^{III}(tpy)_2]$ redox centers, but the self-exchange rate constant $k_{act}^{soln} \approx 10^9\,\mathrm{L\,mol^{-1}\,s^{-1}}$ has been reported for the related $[Ru^{II}/Ru^{III}(bpy)_3]$ system in water.[53] In other words, the measured D_{hop} value corresponds to what is expected for an electron self-exchange involving adjacent redox centers in the transition state.

However, a full coverage of the dendrimer shell would require about $N_{max} \approx 140$ redox centers, so that the average distance between the centers of two $[Ru(tpy)_2]$ molecules on the dendrimer shell is $d(N_{max}/N_0)^{1/2} \approx 2.1$ nm for 64 redox sites. Assuming that electron exchanges occur between $[Ru^{II}/Ru^{III}(tpy)_2]$ redox centers pinned at their equilibrium positions and using an average value of $\lambda = 10\,\mathrm{nm^{-1}}$ (viz., $1\,\mathrm{Å^{-1}}$)[44, 45] should then correspond to $6N_Ak/k_{act}^{soln} \approx 1.2\times10^{-3}$ [Eq. (10)]. However, λ may be as small as $5\,\mathrm{nm^{-1}}$ (viz., $0.5\,\mathrm{Å^{-1}}$), depending on the exact nature of the nonconducting linker which separates the two exchanging centers. The above estimation was based on the maximum reported λ value. Conversely, using the minimum reported value, that is, $\lambda = 5\,\mathrm{nm^{-1}}$ affords $6N_Ak/k_{act}^{soln} \approx 3.5\times10^{-2}$. Since the experimental value of $6N_Ak/k_{act}^{soln}$ is found to be close from unity, both results establish unambiguously that the redox centers are extremely mobile (energetically and dynamically) in their potential wells and may easily achieve close contact at the very moment of electron transfer.

Based on Equation (19), and Figure 2 the equivalent molecular force constant κ maintaining the redox centers in their potential wells must be much less than $10^{-20}\,\mathrm{J\,nm^{-2}}$. Using $\lambda = 10\,\mathrm{nm^{-1}}$, this imposes that $\zeta = 2\lambda^2k_BT/\kappa \gg 25$ so that from Equation (32), $\Omega \ll 10^{-10}$. Conversely, using $\lambda = 5\,\mathrm{nm^{-1}}$, imposes that $\zeta = 2\lambda^2k_BT/\kappa \gg 6$ so that from Equation (32), $\Omega \ll 3.5\times10^{-2}$. Therefore the determination of the maximum surfacic viscosity η_S of one $[Ru(tpy)_2]$ molecule in its potential well depends critically on the value used for λ. Thus, one obtains $\eta_S \ll 10^{-20}\,\mathrm{N\,s\,m^{-1}}$ upon using $\lambda = 10\,\mathrm{nm^{-1}}$ or $\eta_S \ll 5\times10^{-13}\,\mathrm{N\,s\,m^{-1}}$ upon using $\lambda = 5\,\mathrm{nm^{-1}}$. Let us compare these values to that in solution. From the Nernst–Einstein relationship, an average solution diffusion coefficient of $D_{soln} = 5\times10^{-6}\,\mathrm{cm^2\,s^{-1}}$ for a molecule of radius r_m in solution corresponds to a volumic kinematic viscosity $\eta_V = k_BT/(6\pi D_{soln}r_m)$, that is, to an apparent surfacic kinematic viscosity $\eta_s^{app} = \eta_V r_m = 5\times10^{-13}\,\mathrm{N\,s\,m^{-1}}$. This value exceeds the maximum allowable value of η_S determined above. In other words, the mobility of the redox centers on the spherical dendrimeric shell is much larger than that of a free $[Ru(tpy)_2]$ molecule in solution. This may be surprising at first glance since in a dendrimer the $[Ru(tpy)_2]$ centers are connected to radial chains which ought to rub against their neighboring chains to allow any significant displacement of a $[Ru(tpy)_2]$ center. In our view this shows that 1) there is no significant friction between the linkers, and that 2) the dendrimer structure prevents the building-up of a tight solvent and ionic atmosphere around the redox centers as compared with dendrimers in solution.

Since the adsorbed dendrimer structure is more compact than that of a free dendrimer molecule in solution because of the requirement of $\varphi_0 \approx 2\pi/5$, this result is a fortiori valid for similar dendrimers in solution, regardless of the nature of the chemically active center carried at the extremities of the linkers. In other words, this implies that redox centers or catalytic centers linked to a dendritic structure similar to that considered here cross talk much more easily than the same centers when they are free in solution at the same concentration. This is an important effect to take into account for example in the design of dendrimer-supported organometallic catalysts,[23–35] since it establishes unambiguously the existence of a stronger chemical cross-talk than in solution. For example, bimolecular reactions between organometallics catalytic centers that occur with difficulty in solution under catalytic conditions may well become the dominant path when the catalytic centers are supported on a dendritic structure.

Effect of the distribution of dendrimers on the voltammetric oxidation wave

In the above treatment we have relied exclusively on the variations of the voltammetric peak current intensity and potential with the scan rate. However, comparison between the simulated and experimental voltammograms (Figure 4) shows that the predicted voltammetric peaks are sharper than the experimental ones. This is also reflected by the fact that when the dendrimer surfacic concentration is estimated from the limit, $(2.3+0.2)\times10^{-10}\,\mathrm{V\,s^{-1}\,A^{-1}}$, achieved by v/I_p in the smaller scan rates range used in this study (Figure 6a), one obtains $N_deN_0 = (4.4\pm0.5)\times10^{-12}$ C, and since $N_0 = 64$ is known by construction, $\Gamma_d = N_d/(\pi r_0^2N_A) = (0.9\pm0.2)\times10^{-12}\,\mathrm{mol\,cm^{-2}}$ ($r_0 = 5.0\pm0.5\,\mu\mathrm{m}$). When Γ_d is estimated from the charge consumed (from the surface area of the voltammetric peak) one obtains $N_deN_0 = (12\pm2)\times10^{-12}$ C so that $\Gamma_d = (2.5\pm0.4)\times10^{-12}\,\mathrm{mol\,cm^{-2}}$. Both values are consistent with previous more precise determinations of Γ_d ($3.5\times10^{-12}\,\mathrm{mol\,cm^{-2}}$)[8] made for the same dendrimer yet the second evaluation is much closer than that based on the peak current, especially considering that the surface of the platinum electrode used here is much less defined than the electrodes used previously.[8] In other words, it appears that the experimental peak does not correspond to a simple summation of the current peaks due to N_d identical dendrimers, but to the convolution of the individual currents due to a population of different dendrimers.

Let us consider a distribution $G(g)$ of dendrimers which differ by the value of their oxidation potential in the adsorbed state as compared to E^0 in solution: $E^0_{ads}(g) = E^0 + g(RT/F)$. Indeed, even assuming linearized isotherms (that is, $\Gamma_J = \Gamma_J^m[J]_0^{soln}\exp(-\Delta G_J^0/RT)$, where $[J]_0^{soln}$ is the solution concentration of species J = Red,Ox at the interface, Γ_J^m its maximum adsorbed surfacic concentration and ΔG_J^0 its standard free energy of adsorption)[1, 51] for the reduced and oxidized forms of the dendrimer, Equation (88) is valid at equilibrium of the adsorbed phase when the electrode is set at potential E.

$$\Gamma_{Red}/\Gamma_{Ox} = (\Gamma_{Red}^m/\Gamma_{Ox}^m)\exp[(\Delta G_{Ox}^0 - \Delta G_{Red}^0)/RT]([Red]_0^{soln}/[Ox]_0^{soln}) \quad (88)$$

Thus, for a Nernstian couple and $n=-1$ (oxidation wave) Equation (89) is valid, where $E^0_{ads}(g)=E^0+g(RT/F)$ and $g=\ln(\Gamma^m_{Red}/\Gamma^m_{Ox})+(\Delta G^0_{Ox}-\Delta G^o_{Red})/RT$.

$$\Gamma_{Red}/\Gamma_{Ox}=\exp\{F[E^0{}_{ads}(g)-E]\} \quad (89)$$

Equation (89) shows that whenever the $\Gamma_J{}^m$ and $\Delta G^0{}_J$ values differ for the oxidized and reduced forms, $E^0{}_{ads}(g)$ differs from the solution formal potential E^0. Whenever the distribution of g values is not a Dirac function, the voltammetric wave observed in case III-Nernstian for the whole population is given by Equation (90), where $\xi=(F/RT)(E-E^0)$ as defined above, and $G(g)$ is the normalized distribution (the integral of $G(g)$ from g = 0 to infinity is unity) of g values among the whole population of dendrimers adsorbed on the electrode surface.

$$I(\xi)/[N_dN_0e(Fv/RT)]=\int_0^{+\infty}\{\exp(\xi-g)/[1+\exp(g-\xi)]^2\}G(g)dg \quad (90)$$

Figure 7a represents the experimental voltammetric peaks observed at 0.036 and 0.072 MV s^{-1}, that is, when case III-Nernstian is achieved. This presentation eliminates the effect of scan rate so that the two experimental peaks almost coincide. Using the formulation in Equation (90), one may extract the experimental $G(g)$ distribution from these two set of data. $G(g)$ obeys closely a χ^2 distribution law (Figure 7b) [Eq. (91)] with $\sigma_g=1.96$, $\omega=0.41$; $v=1.13$ is the normalization factor corresponding to these σ_g and ω values.

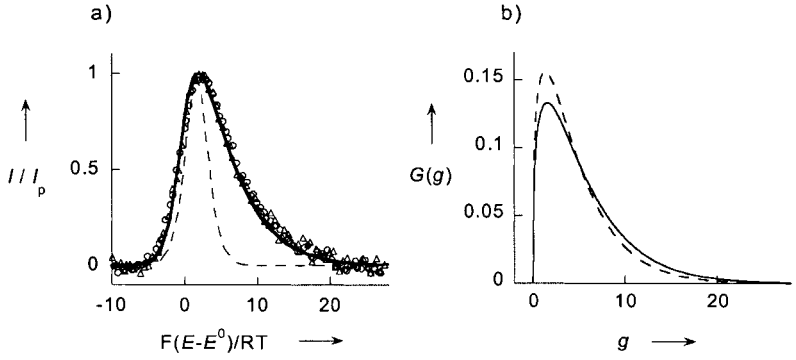

Figure 7. Effect of a population of dendrimers on the overall voltammetric anodic peak observed at the slowest scan rates when the case III-Nernstian kinetic conditions (see Table 1) are obeyed. a) Experimental data corrected from the background base line (circles: $v=0.036$ MV s^{-1}; triangles, $v=0.072$ MV s^{-1}). The thick solid line is the predicted behavior for the population distribution shown by the solid curve in b), while the dashed line is that predicted for a monodisperse distribution ($g_0=1.6$), viz., for $G(g)=\delta(g-1.6)$ where δ is the Dirac function (see text for the definition of g). b) Solid curve: χ^2 distribution of the dendrimer population (reduced state) as a function of g [Eq. (91)] with $\sigma_g{}^{an}=1.96$, $\omega^{an}=0.41$; $v^{an}=1.13$); the maximum of $G^{an}(g)$ corresponds to $g_0{}^{an}=1.6$ and $G^{an}(g_0{}^{an})=0.133$. Dashed curve: χ^2 distribution of the dendrimer population (oxidized state) as a function of $g=|g^{cath}|$ [Eq. (91)] by permuting g into $|g^{cath}|$ with $\sigma_g{}^{cath}=1.67$, $\omega^{cath}=0.41$; $v^{cath}=1.13$); the maximum of $G^{cath}(g)$ corresponds to $g_0{}^{cath}=-1.4$, $G^{cath}(|g_0{}^{cath}|)=0.156$.

The maximum of the $G(g)$ distribution is observed at $g_0=1.6$, that is, to $(\Delta G^0_{Ox}-\Delta G^0_{Red})$ being in the range of about 4 kJ mol^{-1} if one assumes at this stage that $\ln(\Gamma^m_{Red}/\Gamma^m_{Ox})$ is comparatively negligible (sed vide infra). The above σ_g value corresponds to about 5 kJ mol^{-1} for the difference $(\Delta G^0_{Ox}-\Delta G^0_{Red})$. Both values establish that even if the distribution significantly affects the voltammetric peak, it remains extremely narrow (ca., 10%) in view of the adsorption energies involved; for example, $\Delta G^0_{Red}=-(49\pm1)$ kJ mol^{-1} has been determined previously for the adsorption of these dendrimers on platinum electrodes.[8] Again, this conclusion compares satisfactorily with the result of previous STM investigations that have established that these dendrimers give rise to perfectly ordered arrays.[7]

The same distribution [Eq. (91)] was applied to the voltammetric peaks obtained at faster scan rates. This produced reconstructed theoretical voltammetric peaks which compare extremely well with the experimental ones, although only for the lower and upper ranges of scan rates used in this study ($v<0.2$ MV s^{-1}, or $v>1.5$ MV s^{-1}), that is, when the system has reached case III-Nernstian or case I (total charge transfer control). In the intermediate range, one observes a slight but systematic discrepancy between the experimental and reconstructed theoretical voltammograms. In our view, this reflects that the value of g affects to some extent the way by which the system transits from case III-Nernstian to case I-slow charge transfer. In other words, the distribution of g values slightly affects the value of k_S but does not affect D_{hop} and φ_0 in a significant fashion.

Regarding D_{hop} this appears to be a reasonable result since this parameter derives from events that primarily occur far from the electrode surface and therefore characterize the dynamics of the redox centers on the dendrimer shell. This result is also reasonable for φ_0 since, owing to the large adsorption energy of dendrimers ($\Delta G^0_{Red}\approx-50$ kJ mol^{-1}),[8] the effect of the comparatively small distribution of $(\Delta G^0_{Ox}-\Delta G^0_{Red})$, that is, 5 kJ mol^{-1}, is expected to have an extremely modest effect on the geometry of the surface of contact between the electrode and the dendrimer (ca. 10 nm diameter for $\varphi_0\approx2\pi/5$ and $R_0\approx5$ nm). Also, it is rational that even a slight change in adhesion of a dendrimer affects k_S, the heterogeneous rate of electron transfer, since this rate constant is closely related to the coupling between the electrode and the redox centers close to it. However, the effect is modest and shows up mostly in the intermediate range of scan rates where the system experiences a transition between Nernstian and slow charge transfer regimes. From the experimental data obtained in this intermediate range of scan rates, one can extract the distribution of k_S. This was not attempted because the effect is extremely modest ($\sigma_{ks}/k_S<20\%$) compared to that due to g.

© WILEY-VCH Verlag GmbH, D-69451 Weinheim, 2001
0947-6539/01/0710-2222 $ 17.50+.50/0 Chem. Eur. J. 2001, 7, No. 10

Meaning of ΔE_p

Equation (89) predicts an apparent shift of the voltammetric wave with respect to the E^0 value in solution. However, whenever the G distribution does not change upon full oxidation of the adsorbed dendrimers, an identical potential shift should be observed for the reduction wave. In other words, when case III-Nernstian is achieved, both waves should be enlarged and shifted identically with respect to E^0 due to the common distribution of g values, so that they should remain centered around $E^0_{ads}(g_0)$ and ΔE_p should be nearly zero under the case III-Nernstian regime. This is clearly not the case since ΔE_p remains about 80 mV down to very slow scan rates ($v < 100\ mV\,s^{-1}$).[6] Furthermore, Figure 5b shows that the experimental ΔE_p variations versus v are closely reproduced by the theory over the entire range of scan rates used here provided that a constant $\Delta E_p = 80$ mV is added to the theoretical prediction (note that the two points at the highest scan rates deviate because of filtering by the potentiostat and imperfect ohmic drop compensation above $2\ MV\,s^{-1}$). This suggests that the two populations of dendrimers (viz., the completely reduced one versus. the completely oxidized one) experience different G distributions.

The fact that the adsorption behavior differs for the two populations of reduced or oxidized dendrimers is also evidenced by the comparison of the anodic and cathodic voltammetric peaks. Indeed, at the lowest scan rates used here, where the case III-Nernstian regime prevails, the cathodic current peak is about 20% less than the anodic one. One determines a comparable diminution of coverage (ca. 25%) upon considering the relative surface areas of the two voltammetric peaks. Neglecting the possible involvement of charge trapping effects,[6, 54–57] these numbers reflect that in the fully oxidized state the surfacic concentration of dendrimers is about 25% less than that observed in the fully reduced state and that the G distribution is narrower for the fully oxidized state since the diminution in peak current intensity is smaller than that deduced from the area under the peak.

This is a clear indication that one is confronted with a phase transition. One phase prevails when the dendrimers are in their Ru^{II} redox state (this is the one that controls the anodic peak), and another phase prevails when the dendrimers are in their Ru^{III} redox state (this is the one that controls the cathodic peak). Each phase has its own Γ^m value and $G(g)$ distribution. In the following we thus indicate by a superscript 'II' or 'III' the values which pertain to the corresponding phase. The above analysis applies therefore to the Ru^{II} phase which corresponds then to $\Gamma_d{}^{II} = (2.5 \pm 0.4) \times 10^{-12}\ mol\,cm^{-2}$, and obeys a $G^{II}(g)$ χ^2 distribution ([Eq. (91)], Figure 7, solid curve) with a maximum at $g_0{}^{II} = 1.6$, and $\sigma_g{}^{II} = 1.96$, $\omega^{II} = 0.41$, and $v^{II} = 1.13$. The same treatment applied to the Ru^{III} phase (that is, based on the treatment of the cathodic peak, data not shown) shows that $\Gamma_d{}^{III} = 0.75\Gamma_d{}^{II} = (2.0 \pm 0.3) \times 10^{-12}\ mol\,cm^{-2}$. It also obeys a χ^2 distribution, $G^{III}(|g|)$ ([Eq. (91)], Figure 7, dashed curve), with its maximum at $g_0{}^{III} = -1.4$, and $\sigma_g{}^{III} = -1.67$, $\omega^{III} = 0.41$, and $v^{III} = 1.13$. Based on the above analysis, the peak-to-peak separation between the anodic and cathodic voltammetric waves is then given by $\Delta E_p = RT(g_0{}^{II} - g_0{}^{III})/F$. Since $g_0{}^{II} - g_0{}^{III} \approx 3$, the value is predicted to be 76 mV, which compares extremely well to the experimental one of (80 ± 5) mV.

Based on the $g_0{}^{III}$ value determined for the Ru^{III}-phase, one determines $(\Delta G^0_{Ox} - \Delta G^0_{Red})^{III}$ to be about $-3.5\ kJ\,mol^{-1}$, that is, of similar magnitude to $(\Delta G^0_{Ox} - \Delta G^o_{Red})^{II} \approx 4\ kJ\ mol^{-1}$ determined above for the Ru^{II}-phase but with the opposite sign. Note that in the determination of $(\Delta G^0_{Ox} - \Delta G^0_{Red})^{II/III}$ we neglected the contribution of the $\ln(\Gamma^m_{Ox}/\Gamma^m_{Red})^{II}$ or $\ln(\Gamma^m_{Ox}/\Gamma^m_{Red})^{III}$ terms in each phase since we have no way to determine them at present. However, since $(\Gamma^m_{Ox})^{III}/(\Gamma^m_{Red})^{II} \approx 0.75$ one expects that $\Gamma^m_{Ox}/\Gamma^m_{Red}$ is even closer to unity in each phase so that the resulting error should be negligible and, in any case, much lower than the widths of each distribution as determined from the corresponding σ_g values (about 5 and $-4.5\ kJ\,mol^{-1}$ for the Ru^{II} and Ru^{III} phases respectively). In other words, the oxidized dendrimer molecules are more strongly adsorbed than their reduced form in the fully oxidized Ru^{III} phase, while the reverse is observed in the fully reduced Ru^{II} phase.

Such a phase transition is expected for highly ordered arrays such as those produced by these dendrimers.[7] Indeed, because of electroneutrality, full oxidation of one dendrimer molecule requires the presence of 64 BF_4^- anions from the supporting electrolyte around the dendrimer shell. This suffices to give a about 5% increase in its apparent radius. However, dipole–dipole repulsions then occur between adjacent oxidized dendrimers so that the apparent increase in radius must be larger than this number in order to allow adequate screening of electrostatic repulsions by the ionic atmosphere. Both phenomena may then very well account for the overall apparent increase by about 10–15% of the radius (note that such an increase in radius results in an increase in area of about 25% which, in turn, is reflected in a similar diminution in the surface coverage). The resulting increase in radius explains, therefore, why the highly ordered array of the Ru^{II} phase resists the insertion of oxidized dendrimers into it. Similarly, reduction taking place within a highly ordered array of oxidized dendrimers in the Ru^{III} phase should require energy to compensate the creation of an uncovered area of the electrode in the middle of the Ru^{III} array. This suggests that $(\Delta G^0_{Ox} - \Delta G^0_{Red})^{II}$ or $(\Delta G^0_{Ox} - \Delta G^0_{Red})^{III}$ do not reflect variations of binding energies between the dendrimers and the electrode surface, but rather, the energetics of the defects created in either ordered array by the creation of dendrimer molecules of a different redox state.

The maximum interaction between adjacent sites in either array is expected to occur at the level of the equatorial planes of the adsorbed dendrimers. Since $\varphi_0 \approx 2\pi/5$, the dendrimers rest nearly on their equatorial plane (compare Figure 1b) so that such repulsions are expected to occur at near maximum strength as soon as only a few percent of the redox sites borne by a dendrimer have changed redox state. This explains therefore *a posteriori* why D_{hop} and φ_0 are almost unaffected by the distribution of g, and why k_S is only slightly affected. Similarly, this also explains why one needs to add the same constant term (80 mV) to the predicted $\Delta E_p{}^{th}$ values irrespective of the scan rate in order to reconcile the predicted and experimental ΔE_p (Figure 5b).

The existence of two different phases requires that the population of adsorbed dendrimer must experience phase transitions upon oxidation/reduction cycles. Previous investigations by quartz microbalance (though with ClO_4^- supporting electrolyte anion instead of BF_4^- used here) clearly established the occurrence of a perfectly reproducible mass hysteresis during the oxidation/reduction cycles.[6] The mass mid-point transition occurred near the end of the voltammetric peak during the anodic scan ($v = 50\ mV\ s^{-1}$), while it occurred in conjunction with the reduction peak during the cathodic scan. This behavior is consistent with different $(\Delta G^{=}_{Ox} - \Delta G^{=}_{Red})$ values in each phase as inferred from the present analysis.

In our view, this conclusion explains, also a posteriori, the experimental observation that we made with the amorphous electrodes used in this study compared to what occurs on much better defined platinum surfaces.[6–8] Indeed, as explained before, we noted that the electrode needed to be cycled numerous times before sharp voltammetric signals could be observed. In fact, the first voltammetric cycles gave rise to rather sluggish anodic and cathodic waves, which progressively sharpened upon cycling to yield, reproducibly, those shown and used here. When this final reproducible state was achieved, the voltammetric system did not evolve with time except when the electrode was repolished. So each voltammogram presented and used here was obtained in a single scan mode after this *pre*treatment and yielded reproducible results from run to run. In view of what has been described above, one may then consider that when a fresh polished surface is introduced into the dendrimer solution, dendrimers (in their reduced form) adsorb kinetically onto the amorphous platinum electrode surface. This may well lead to a series of kinetic microdomains characterized by their own g_0^{II} and σ_g^{II} values so that the first voltammetric waves observed appear sluggish. Upon cycling continuously anodically and cathodically the electrode, one anticipates continuous desorption-adsorption cycles to occur because of the alternative change of sign in $(\Delta G^{=}_{Red} - \Delta G^{=}_{Red})$ since the active phase in each half-cycle differs. This continuous desorption–adsorption process is then expected to "anneal" the initial broad distribution by imposing ultimately a thermodynamic situation, so that the distribution of g values should sharpen so as to give, ultimately, those presented in Figure 7b.

Conclusion

We have shown here, thanks to the possibility of performing cyclic voltammetry in the megavolt-per-second range of scan rates, that the extension of a diffusion layer can be tuned to fit precisely the nanometric dimensions of an electroactive nanoobject. In this study we applied this ultrafast voltammetric method to the study of electron-hopping diffusion within a dendrimer structure bearing redox sites on its external shell. Owing to the topology of such particular structure the voltammetric behavior of such objects obey new specific diffusional patterns that reflect the specific topological arrangement of the redox sites onto the dendrimer shell. These specific behaviors complicate significantly the voltammetric analysis, yet in return they afford a precise description of the shape of the adsorbed dendrimers. This is a unique result which could not be achieved by STM or atomic force microscopy (AFM) exploration of the same system, since either method gives access to only that part of the adsorbed globule that is exposed to the solution,[7] in this case, above the equatorial plane of the adsorbed dendrimers. Conversely, the ultrafast voltammetric investigation affords a precise description of the region facing the electrode, that is, of the part located *below* the equatorial plane. It was thus established that the contact area between the dendritic structure and the electrode is quite large, which is in agreement with the large adsorption energies reported previously by some of us.[8] In fact, the adsorbed dendrimer structure is then distorted[36–38] and resembles more closely a hemisphere resting onto the electrode than a spherical globule as it should be in solution (Figure 1b). In our view this ability to provide a sound topological information is a new and unique property of voltammetric exploration of electroactive nanoobjects.

Besides such topological information, the voltammetric investigation gave access to the measurement of the electron-transfer self-exchange rate constant between the $[Ru^{II}/Ru^{III}(tpy)_2]$ redox sites borne by the dendritic structure. Surprisingly, we observed this rate constant to be comparable with electron transfer occurring between redox centers in contact, albeit the average distance between their centers is about 2 nm. This indicates that the redox centers are extremely mobile around their equilibrium position. The model that has been developed here establishes that this may occur only if the kinematic viscosity of the centers is smaller than that of the same centers in solution. This highlights the extreme mobility of dendritic structures and the extremely facile cross-talk between centers borne by dendrimers similar to that studied here. This important effect which to the best of our knowledge has never been shown before needs to be taken into account in the design of dendrimer-supported organometallic catalysts,[23–35] since this may induce different mechanistic paths than those observed for the same homogeneous catalytic centers.

Finally, the knowledge of the independent behavior of each dendrimer unit has allowed the statistical treatment of the whole population of dendrimers adsorbed onto the electrode surface. Interestingly this part of our study allowed us to establish that a rather narrow distribution may nevertheless affect considerably the shape of the voltammetric waves vis a vis a monodisperse population. In particular, the simple model developed here easily accounts for the existence of the potential difference between the anodic and cathodic peak at small scan rates by an energetic hysteresis due to the fact that each given array of adsorbed dendrimers, that is, an arrray of reduced or oxidized molecules, accepts with considerable difficulty a redox change of its components. To the best of our knowledge this is the first time that such phenomenon has been properly identified by electrochemistry of bidimensional arrays.

© WILEY-VCH Verlag GmbH, D-69451 Weinheim, 2001
0947-6539/01/0710-2224 $ 17.50+.50/0 *Chem. Eur. J.* **2001**, *7*, No. 10

Experimental Section

The dend-64-[$Ru^{II}/Ru^{III}(tpy)_2$] dendrimer investigated in this study (see Scheme 1) was synthesized and characterized according to reported procedures.[6–8]

The home-made ultrafast potentiostat equipped with feedback electronic compensation used in this study has been described in full details elsewhere.[4] Its bandpass in the full compensation mode resulted in no significant distortion of the voltammograms up to 2 $MV\,s^{-1}$.[4] Above this scan rate the potentiostat introduced slight distortions of the voltammetric peaks (compare Figure 5b).[4] Under this scan rate it introduced only a constant time lag of 20 ns that was eliminated by numerical shift of the digitally recorded current-times curves.[4]

The three-electrode electrochemical cell (0.3 mL) and other electronic apparatus used in this study were identical to those previously reported.[4] The working electrode was a platinum disk of 5.0 ± 0.5 μm radius made by the cross-section of a platinum wire (Goodfellow) of 5 μm nominal radius sealed into soft glass, polished and calibrated according to reported procedures.[58] It was polished on alumina 0.3 μm (Presi) before use. The counter electrode was a platinum wire and the reference electrode a floating *pseudo*reference electrode as described elsewhere.[4] The size of the three electrodes and of their leads were critical so the cell was mounted directly into the potentiostat board to minimize the stray capacitances.[4] The cell was filled with 0.25 mL of a saturated solution of the dend-64-[$Ru^{II}/Ru^{III}(tpy)_2$] dendrimer[6–8] in acetonitrile, distilled before use and stored under argon, and containing 0.6 M NEt_4BF_4 (Aldrich) that was dried under vacuum for 3 h prior to the experiment. During all experiments, the cell was kept under an argon blanket.

The first voltammetric scans with a freshly polished electrode gave broad voltammetric cycles. However, cycling the electrode anodically and cathodically progressively resulted in reproducible sharper voltammetric peaks. After this preparation phase of the electrode, there was no need to reproduce this pretreatment unless the electrode was disconnected from the cell and polished again. Each voltammogram used here (Figure 4) was obtained in the single scan mode. Five ($v > 0.1\,MV\,s^{-1}$) or 20 ($v \leq 0.1\,MV\,s^{-1}$) independent voltammograms were averaged to increase the signal-to-noise ratio without introducing any significant distortion of the voltammetric waves.

All the programs developed in this work were written in language C^{++} and ran on a PC-Pentium 333 MHz. They were built using classical implicit finite difference algorithms,[59] based on the dimensionless system of Equations (40), (42), (71) – (73) . The current was then obtained by application of Equation (76). The programming was classical for such implicit algoritms except for a very critical point related to the value of the mesh of the space grid. For this, for any given value of φ_0, β [Eq. (75)] and Λ [Eq. (76)] the maximum extent of the diffusion layer was roughly estimated by application of $\eta_{diff} = 5/\Psi(\xi_{max})$ based on the theoretically predicted limiting dimensionless currents Ψ derived analytically in this work and on the schematic zone diagram shown in Figure 3a. The ensuing diffusion layer was then equally separated into 50 space elements to define the mesh grid for the calculations. It was checked that increasing η_{diff} by a factor two to five while keeping the same space interval did not resulted in any noticeable change of the computed dimensionless current. When, η_{diff} exceeded the value $\eta_{diff}^{\pi/2}$ corresponding to $\varphi = \pi/2$, the calculation was performed with two connected space grids. For $\eta \leq \eta_{diff}^{\pi/2}$ (viz., for $\varphi_0 \leq \varphi \leq \pi/2$) the calculation was performed in the η space [Eq. (39)] and the diffusion equation was Equation (40) with D^* defined as in Equation (42). For $\varphi > \pi/2$, the calculations were performed directly into the φ space to save computation time, so that Equation (35) was solved instead. The interconnection between the two spaces was ensured by forcing continuity conditions on f and $\partial f/\partial\eta$ (viz., $\partial f/\partial\eta = (\partial f/\partial\varphi)(\beta\sin\varphi)/2$, viz., $\partial f/\partial\eta = \beta(\partial f/\partial\varphi)/2$ at $\pi/2$) at $\eta = \eta_{diff}^{\pi/2}$ (viz., at $\varphi = \pi/2$). The validity of the program was tested by forcing extreme conditions on φ_0, Λ, or β, so that the system was shifted in any of the six limiting cases delineated in this study, and by checking then that it produced then the appropriate predicted limiting dimensionless currents within a precision better than 0.1 %. This ensured that the simulations were performed with an excellent precision in the general case and in any transition between limiting behavior (Figure 3) as well as under any conditions required for the analysis of the present experimental data.

Acknowledgement

In Paris this work was supported in parts by CNRS (UMR 8640 "PASTEUR"), Ecole Normale Supérieure, and the French Ministry of Research and Education (MENRT ; Action Spécifique DGRT no. 97.1502). The work at Cornell University was supported by the Office of Naval Research and the Cornell Center for Materials Research.

[1] A. J. Bard, L. R. Faulkner, *Electrochemical Methods*, Wiley, New York, **1980**.
[2] C. Amatore in Physical Electrochemistry, (Ed.: I. Rubinstein), M. Dekker, New York, **1995**, Chapter 4.
[3] C. Amatore, E. Maisonhaute, G. Simonneau, *Electrochem. Commun.* **2000**, *2*, 81.
[4] C. Amatore, E. Maisonhaute, G. Simonneau, *J. Electroanal. Chem.* **2000**, *486*, 141.
[5] C. Amatore, C. Lefrou, *J. Electroanal. Chem.* **1990**, *296*, 335.
[6] G. D. Storrier, K. Takada, H. D. Abruña. *Langmuir*, **1999**, *15*, 872.
[7] D. J. Díaz, G. D. Storrier, S. Bernhard, K. Takada, H. D. Abruña, *Langmuir*, **1999**, *15*, 7351.
[8] K. Takada, G. D. Storrier, M. Morán, H. D. Abruña. *Langmuir*, **1999**, *15*, 7333.
[9] K. Takada, D. J. Diaz, , H. D. Abruña, I. Cuadrado, C. Casado, M. Morán, J. Losada, *J. Am. Chem. Soc.* **1997**, *119*, 10763.
[10] B. Alonso, I. Cuadrado, M. Morán, J. Losada, *J. Chem. Soc. Chem. Commun.* **1994**, 2575.
[11] E. Alonso, C. Valerio, J. Ruiz, D. Astruc, *New J. Chem.* **1997**, *21*, 1139.
[12] I. Cuadrado, M. Morán, C. M. Casado, B. Alonso, F. Lobete, B. Garcia, M. Ibisate, J. Losada, *Organometallics*, **1996**, *15*, 5278.
[13] B. Alonso, M. Morán, C. M. Casado, F. Lobete, J. Losada, I. Cuadrado, *Chem. Mater.* **1995**, *7*, 1440.
[14] S. S. Sheiko, G. Eckert, G. Ignat′eva, A. M. Muzafarov, J. Spikerman, H. J. Räder, M. Möller, *Macromol. Rapid Commun.* **1996**, *17*, 283.
[15] R. W. Murray, *Phil. Trans. R. Soc. London* **1981**, *A. 302*, 253.
[16] H. J. Dahms, *J. Phys. Chem.* **1968**, *72*, 362.
[17] I. Ruff, V. J. Friedrich, *J. Phys. Chem.* **1971**, *75*, 3297.
[18] I. Ruff, V. J. Friedrich, K. Demeter, K. Csillag, *J. Phys. Chem.* **1971**, *75*, 3303.
[19] C. P. Andrieux, J. M. Savéant, *J. Electroanal. Chem.* **1980**, *111*, 377.
[20] E. Laviron, *J. Electroanal. Chem.* **1980**, *112*, 1.
[21] D. N. Blauch, J. M. Savéant, *J. Am. Chem. Soc.* **1992**, *114*, 3323.
[22] D. N. Blauch, J. M. Savéant, *J. Phys. Chem. 97*, **1993**, 6444.
[23] D. A. Tomalia. *Adv. Mater.* **1994**, *6*, 529.
[24] G. R.Newkome, C. N.Moorefield, F. Vögtle, *Dendritic Molecules: Concepts, Syntheses, Perspectives*, VCH, Weinheim, **1996**.
[25] F. Zeng, S. C. Zimmerman. *Chem. Rev.* **1997**, *97*, 1681.
[26] J. S. Moore. *Acc. Chem. Res.* **1997**, *30*, 402.
[27] O. A. Matthews, A. N. Shipway, J. F. Stoddart, *Prog. Polym. Sci.* **1998**, *23*, 1.
[28] H. Frey, C. Lach, K. Lorenz. *Adv. Mater.* **1998**, *10*, 279.
[29] C. Gorman, *Adv. Mater.* **1998**, *10*, 295.
[30] D. A. Tomalia, A. M. Naylor, W. A. Goddard, III, *Angew. Chem.* **1990**, *102*, 119; *Angew. Chem. Int. Ed. Engl.* **1990**, *29*, 138.
[31] J. M. Fréchet, *Science*, **1994**, *263*, 1710.
[32] P. Bhyrappa, J. K. Young, J. S. Moore, K. S. Suslick, *J. Am. Chem. Soc.* **1996**, *118*, 5708.
[33] P. J. Dandliker, F. Diederich, M. Gross, C. B. Knobler, A. Louati, E. M. Sanford, *Angew. Chem.* **1994**, *106*, 1821; *Angew. Chem. Int. Ed. Engl.* **1994**, *33*, 1739.
[34] J. W. J. Knapen, A. W. van der Made, J. C. de Wilde, P. W. N. M. van Leeuwen, P. Wijkens, D. M. Grove, G. van Koten, *Nature*, **1994**, *372*, 659.
[35] A. Miedaner, C. J. Curtis, R. M. Barkley, D. L. DuBois, *Inorg. Chem.* **1994**, *33*, 5482.
[36] M. Zhao, H. Tokuhisa, R. M. Crooks, *Angew. Chem.* **1997**, *109*, 614; *Angew. Chem. Int. Ed. Engl.* **1997**, *36*, 596.
[37] H. Tokuhisa, M. Zhao, L. A. Baker, V. T. Phan, D. L. Dermody, M. E. Garcia, R. F. Peez, R. M. Crooks, T. M. Mayer, *J. Am. Chem. Soc.* **1998**, *120*, 4492.

[38] A. Hierlemann, J. Campbell, L. A. Baker, R. M. Crooks, A. J. Ricco, *J. Am. Chem. Soc.* **1998**, *120*, 5323.
[39] C. P. Andrieux, J. M. Savéant in *Molecular Design of Electrode Surfaces*, (Ed.: R. W. Murray), Wiley, New York, **1992**, Chapter 5.
[40] M. Majda in *Molecular Design of Electrode Surfaces* (Ed.: R. W. Murray), Wiley, New York, **1992**, Chapter 4.
[41] C. Amatore, B. Fosset, J. E. Bartelt, M. R. Deakin, R. M. Wightman, *J. Electroanal. Chem.* **1988**, *256*, 255.
[42] J. M. Savéant, *J. Electroanal. Chem.* **1988**, *242*, 1.
[43] *Tunneling in Biological Systems*, (Eds.: B. Chance, D. D eVault, H. Frauenfelder, R. A. Marcus, J. R. Schrieffer, N. Sutin), Academic Press, New York, **1979**.
[44] S. Mayo, W. R. Ellis, R. J. Crutchley, H. B. Gray. *Science*, **1986**, *233*, 948.
[45] C. J. Miller in *Physical Electrochemistry* (Ed.: I. Rubinstein), M. Dekker, New York, **1995**, Chapter 2, and references therein.
[46] M. Von Smoluchowski, *Ann. Phys.* **1915**, *48*, 1103.
[47] R. A. Marcus, *Discuss. Faraday Soc.* **1960**, *129*, 21.
[48] R. M. Noyes, *J. Chem. Phys.* **1954**, *22*, 1349.
[49] C. A. Amatore, M. R. Deakin, R. M. Wightman, *J. Electroanal. Chem.* **1986**, *207*, 23.
[50] C. Amatore, B. Fosset, *Anal. Chem.* **1996**, *68*, 4377.
[51] E. Laviron in *Electroanalytical Chemistry*, *Vol. 12* (Ed.: A. J. Bard), M. Dekker, New York, **1982**, pp. 53 – 112.
[52] L. Nadjo, J. M. Savéant, *J. Electroanal. Chem.* **1973**, *48*, 113.
[53] N. Sutin, C. Creutz, *Pure Appl. Chem.* **1980**, *52*, 2717.
[54] H. D. Abruña, P. Denisevich, M. Umaña, T. J. Meyer, R. W. Murray, *J. Am. Chem. Soc.* **1981**, *103*, 1.
[55] P. Denisevich, K. W. Willman, R. W. Murray, *J. Am. Chem. Soc.* **1981**, *103*, 4727.
[56] K. W. Willman, R. W. Murray, *J. Electroanal. Chem.* **1982**, *133*, 211.
[57] P. G. Pickup, W. Kutner, C. R. Leidner, R. W. Murray, *J. Am. Chem. Soc.* **1984**, *106*, 1991.
[58] C. Amatore, S. Szunerits, L. Thouin, *Electrochem. Commun.* **2000**, *2*, 248.
[59] J. Crank, *Mathematics of Diffusion*, Claredon Press, London, **1964**.

Received: November 6, 2000 [F2849]

 © WILEY-VCH Verlag GmbH, D-69451 Weinheim, 2001 0947-6539/01/0710-2226 $ 17.50+.50/0